

Politecnico di Torino

FACOLTÀ DI INGEGNERIA

Corso di Laurea Magistrale in Ingegneria Elettrica



Comprehensive comparison of coil topologies for inductive power transfer systems for automotive applications

Candidato:
Calogero Gruttad'Auria

Relatori:
Prof. Fabio Freschi
Ing. Vincenzo Cirimele

Abstract

In the recent years, there has been a growing interest in electric vehicles (EVs) for future sustainable mobility. EVs present several advantages such as high efficiency, low maintenance, absence of pollutant emissions. However, there are several unsolved problems related to the battery. Induction power transfer (IPT) is a technology that can solve one major issue related to the vehicle autonomy. IPT allows to charge the vehicle battery without any electric contact by using the magnetic coupling between two coils one placed on ground and a second one installed under the EV. The charge can be either static or dynamic i.e. with vehicle stopped or while it is moving. As this technology is still under development, there are many open issues. One of these is related to the shape of the coils. This thesis focuses on the analysis of the electromagnetic properties of the different coil shapes proposed in the current scientific literature by performing a systematic comparison to highlight the main properties of each topology. The evaluation is conducted under repeatable conditions proposed and discussed in this work. The comparison is then provided by analysing the most representative parameters able to describe pros and cons of each coil topology considering representative working conditions. The results of the comparison are presented and discussed.

Acknowledgement

Il mio percorso universitario volge al termine, pertanto ritengo doveroso ringraziare alcune persone che mi hanno accompagnato in questi anni.

Desidero ringraziare il Prof. Fabio Freschi per avermi proposto un interessante argomento da trattare e avermi fornito il suo sostegno scientifico durante lo sviluppo della tesi.

Ringrazio l'Ing. Vincenzo Cirimele che mi ha seguito lungo tutto il periodo di tesi. Lo ringrazio per essere sempre stato disponibile al confronto e per i suoi consigli in tutte le fasi cruciali della tesi.

Il ringraziamento più grande va alla mia famiglia. Ringrazio i miei genitori non solo per il sostentamento economico datomi in questi anni. Li voglio ringraziare per aver creduto sempre in me, soprattutto nei momenti difficili, non hanno mai dubitato e mi hanno sempre spronato a dare il meglio. Li ringrazio per avermi dato la possibilità di studiare e di avermi dato sempre il loro appoggio nel sostenere le mie scelte. Ringrazio mia sorella per il suo essere amica prima che sorella. Ha sempre fatto tutto il possibile, offrendomi il suo sostegno nelle decisioni importanti e il suo aiuto nelle situazioni di difficoltà. La ringrazio per avermi incoraggiato a conseguire questo obiettivo e per i momenti belli passati insieme in questi anni. Infine, voglio ringraziare i miei nonni per i loro saggi consigli e i loro insegnamenti che porto sempre con me.

Contents

1	Introduction	5
1.1	Introduction	5
2	Basic principles of IPT systems	7
2.1	Main characteristics of IPT systems	7
2.2	Circuit modeling	8
2.3	Compensation topologies	9
2.4	Hybrid topologies	11
2.5	Efficiency	12
2.6	Conclusion	13
3	State of the art	14
3.1	State of the art	14
3.2	Circular geometry	14
3.3	Rectangular coil types	19
3.4	Considerations	27
4	Comparison	29
4.1	Introduction	29
4.2	Coil layout criteria	29
4.3	Evaluation parameters	33
4.3.1	Coupling coefficient k	33
4.4	Coupling coefficient of IPT	36
4.4.1	Unipolar coils	36
4.4.2	Polarized coils	37
4.4.3	Double-D quadrature coil	40
4.4.4	Additional geometries	42
4.4.5	Coupling factor k representation	45
4.5	Magnetic flux density B	48
5	Comparison results	52
5.1	Comparison results	52
5.2	Coupling factor k	52
5.2.1	No misalignment	52
5.2.2	Values of k varying the air-gap	53
5.2.3	Coils behavior to x misalignment	54
5.2.4	Coils reaction to y misalignment	56
5.3	Magnetic flux density B	57
5.3.1	Normalized B values	57

5.3.2	B field on x direction transmitter plane	63
5.3.3	B field on x direction central plane	64
5.3.4	B field on x direction receiver plane	65
5.3.5	B field on y direction transmitter plane	66
5.3.6	B field on y direction central plane	67
5.3.7	B field on y direction receiver plane	68
5.4	3D B field representation on x-z and y-z planes	69
6	Conclusion	72
6.1	Coupling factor k	72
6.2	Magnetic flux density B	72
A	Appendix	74
	Bibliography	78

Chapter 1

Introduction

1.1 Introduction

The world of mobility is changing year by year. The number of electric vehicles (EVs) is increased in the last years and this trend is intended to increase in the future. The electric cars have different advantages with respect to the internal combustion engines powered vehicles, such as: high efficiency, less acoustic noise and no pollutant gas emissions. The main EVs drawback are related to the battery. This latter has lower energy density with respect to the usual fossil fuels. For this reason EVs have a limited autonomy and need for more frequent charges. Currently, the EVs are charged in charging station using a plugging a cable. The main cons of this method is the long charging time needed with respect to refuel time. The inductive power transfer (IPT) is a solution that allows to overcome this drawback. The IPT system relies on the possibility to transfer electric energy to the EV using two coils magnetically coupled. One coil is placed on the ground and is called transmitter; another coil is mounted on board the EV and is called receiver. This system offers two different ways to charge: static and dynamic. The first one, allows to charge the EV simply parking it on the transmitter coil. Its typical applications are: parking lot and private garage. The second one allows to charge the EV while they are in motion. This second solution is particularly suitable to improve the EVs autonomy in order to reduce its dependence on the battery.

In these years, several coil geometries have been proposed in order to improve the system performances. Some of the proposed geometries are widely used with respect to others, but each of them present pros and cons. This thesis aims to make a comparison between these coil topologies under fixed evaluation criteria. The coils are evaluated using two IPT important parameters: the coupling factor k and the magnetic flux density B .

This thesis is arranged as follow:

The first chapter, explain the basic principles on which is based the IPT technology. An equivalent circuit, is adopted to introduce the system equations and the coupling factor k . There is also a section dedicated to the compensation topologies, explaining what advantages and disadvantages has each of them. The last section reports the expression of the system efficiency.

The second chapter, analyses the most important studies taken into account in this thesis. The chapter is composed by two sections. The first one reports all the studies on the circular type geometry. While, the second section, reports all the rectangular type coils, including the polarized ones.

The third chapter, introduces and describes the evaluation criteria at the base of the comparison. Finally, the chosen performance parameters (k and B), are discussed together with the adopted method for their computation.

The results of the comparison are reported in chapter four.
Some conclusion and future improvements of the work are presented in chapter five.

Chapter 2

Basic principles of IPT systems

This chapter introduces the basic principles of the induction power transfer (IPT) systems. First, is introduced a general view of the entire system and secondly are explained the basic system principles using a circuit model. Finally, the compensation topologies and the system efficiency are discussed.

2.1 Main characteristics of IPT systems

Electricity is one of the most common energy vector. Since the late 19th century, the first experiments made by Faraday on electromagnetic induction in 1832, the application on radio frequencies made by Herz in 1895 and Tesla's experiments in the first years of the 20th century, proved the possibility to transmit energy in a wireless mode, opening a wide field of research. The scientific community has gathered all the different technologies to transfer energy without electric contact under the definition wireless power transfer (WPT). The inductive power transfer (IPT) is a special category of the WPT technology.

An IPT system relies on the same electromagnetic laws of a WPT system: the Ampere and Faraday laws. Although, an IPT system has need of two further conditions to works:

- The use of high frequency to improve the power transfer capability
- The use of capacitors connected to the coils to create a resonant system, improving the power transmission

This thesis is focused on IPT systems for EVs. A general block diagram that reports the main system elements is depicted in 2.1

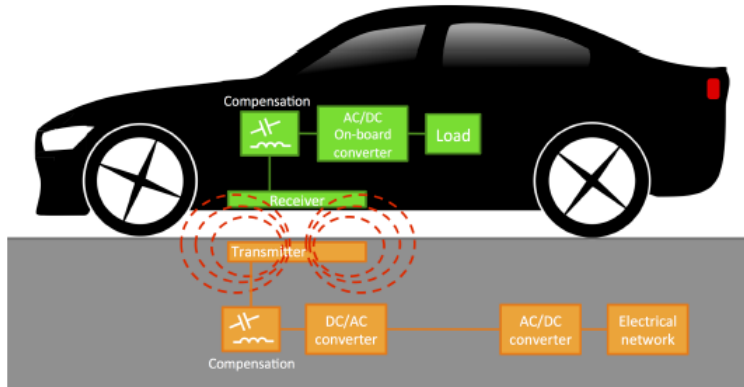


Figure 2.1: Block diagram that reports the basic elements of the IPT system [2]

An IPT system is composed by a fixed coil, called transmitter, and a coil placed under the vehicle chassis called receiver. The transmitter is powered by an inverter that provides a high frequency (tens of kilohertz) current to generate a high frequency field. This field, linking the receiver, is able to transfer electrical power toward the vehicle. In the end, the receiver induced current have to be rectified to charge the battery.

This technology has a series of advantages:

- For a static application, e.g parking lot, this technology is able automatically charges the vehicle. There is no need to insert the plug, no external installation are required, the safety is increased and the possibility of vandalism is reduced.
- The system is protected from adverse environmental conditions, such as: snow, water, dirt and chemicals
- The system have no mechanical contacts, this allows to reduce maintenance costs with a longer life cycle

Another possible application is the dynamic charging, that allows to charge the vehicle while it is moving. This dynamic IPT aims to eliminate the time needed to stop the vehicle for charging, increasing the vehicle autonomy.

2.2 Circuit modeling

In this section, the equivalent model of system will be discussed. An IPT system can be seen as: an energized coil (transmitter) coupled with a second coil (receiver) that supply an electric load. Therefore, an equivalent circuit can be proposed, as in 2.2

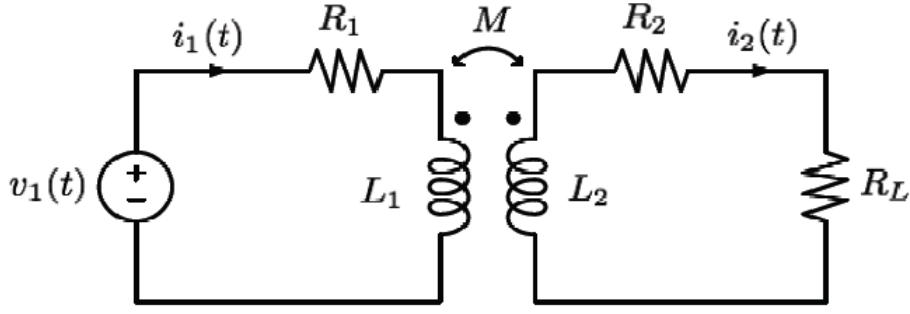


Figure 2.2: IPT equivalent circuit model [1]

where:

- R_1 and R_2 are respectively the transmitter and the receiver winding resistance
- L_1 and L_2 are respectively the self-inductance of the transmitter and the receiver
- M is the mutual inductance between the coils, it can be demonstrated that, if the system is symmetric, M is equal for both windings

These parameters allow to define the coupling factor k . It is an important parameter that is helpful to understand how much flux, generated by the transmitter, links with the receiver

$$k = \frac{M}{\sqrt{L_1 L_2}} \quad (2.2.1)$$

It is a geometry related parameter and its value is included between:

$$0 \leq k \leq 1 \quad (2.2.2)$$

2.3 Compensation topologies

In the previous paragraph has been discussed the necessity of of the IPT system to being compensated. Two coils coupled in the air without any compensation would lead to a loosely coupled system, with a low power transferred from transmitter to receiver. The compensation is useful to improve the transmission of power between the coils of the system. The system can be described by the phasor equations:

$$\begin{cases} \hat{V}_1 = R_1 \hat{I}_1 + j\omega L_1 \hat{I}_1 - j\omega M \hat{I}_2 \\ j\omega M \hat{I}_1 = R_2 \hat{I}_2 + j\omega L_2 \hat{I}_2 + R_L \hat{I}_2 \end{cases} \quad (2.3.1)$$

On the primary side the compensation is applied to minimize the VA power supply and to have zero phase. The term ωL_1 implies an apparent power S_1 higher than the active power P_1 . On the receiver side, the compensation is useful to have the maximum power transfer. In fact, the impedance ωL_2 increase with the increasing of the frequency, reducing the I_2 current that flows in the receiver coil. This fact limit the transferred power.

Therefore, is important to compensate both sides of the system, in order to satisfy the upper conditions. This allows to reduce the switching losses of the power electronics system and to achieve a constant current and a constant voltage charging.

There are four basic compensation topologies, as reported in fig. 2.3:

- a) STR: series transmitter and receiver compensation
- b) STPR: series transmitter and parallel receiver compensation
- c) PTSR: parallel transmitter and series receiver compensation
- d) PTR: parallel transmitter and receiver compensation

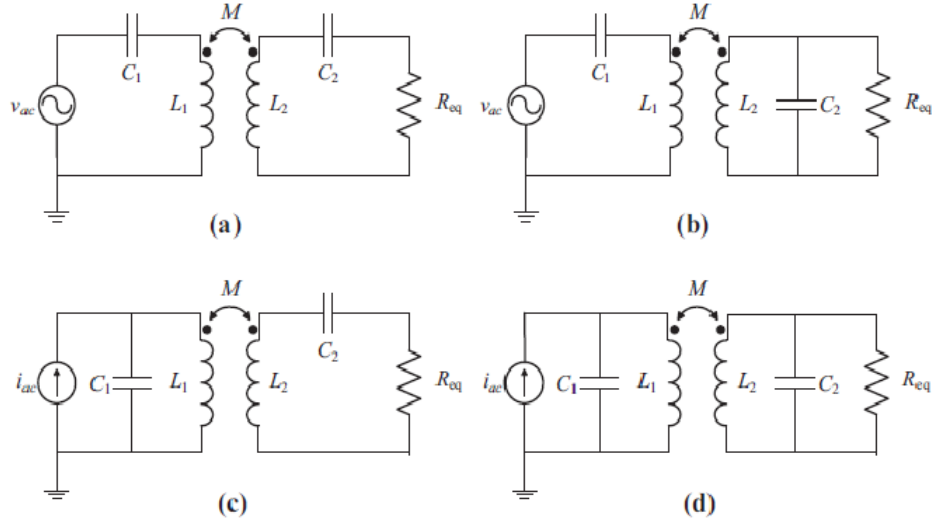


Figure 2.3: Compensation topologies: (a) STR; (b) STPR; (c) PTSR; (d) PTR [3]

It has been already said that the capacity compensation at the receiver part is used to maximize the power transferred. From the basic definition of a resonant circuit it can be written:

$$\omega^2 L_2 C_2 - 1 = 0 \quad (2.3.2)$$

the capacity that fulfill the resonant condition at the *resonant angular frequency* ω_0 is:

$$C_2 = \frac{1}{\omega_0^2 L_2} \quad (2.3.3)$$

In order to achieve a right compensation C_1 must be chosen to compensate the self-inductance of the system and the imaginary component of \hat{Z}_R at the same resonant frequency of the receiver. \hat{Z}_R can be written as:

$$\hat{Z}_R = \frac{\omega^2 M^2}{Z_R} \quad (2.3.4)$$

this expression highlight that the type of compensation is linked with the receiver topology.

Considering a parallel compensating receiver, \hat{Z}_2 can be written as:

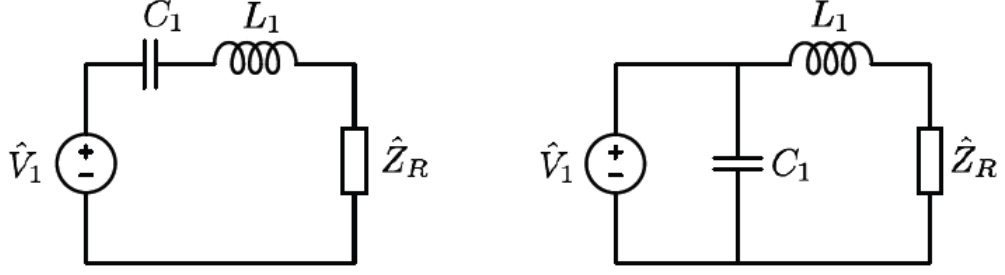


Figure 2.4: a) series compensated transmitter b) parallel compensated trasmitter [1]

$$\hat{Z}_2 = j\omega L_2 + \frac{R_L}{1 + j\omega_0 R_L C_2} \quad (2.3.5)$$

then \hat{Z}_R will be:

$$\hat{Z}_R = \frac{\omega_0^2 M^2}{j\omega_0 L_2 + \frac{R_L}{1 + j\omega_0 R_L C_2}} \quad (2.3.6)$$

The C_1 expressions are[1]:

$$\left\{ \begin{array}{l} C_1^{STR} = \frac{1}{\omega^2 L_1} \\ C_1^{STPr} = \frac{1}{\omega_0^2 \left(L_1 - \frac{M^2}{L_2} \right)} \\ C_1^{PTSR} = \frac{L_1}{\left(\frac{\omega_0^2 M^2}{R_L} \right) + \omega_0^2 L_2} \\ C_1^{PTR} = \frac{L_1 - \frac{M^2}{L_2}}{\left(\frac{M^2 R_L}{L_2} \right) + \omega_0^2 \left(L_1 - \frac{M^2}{L_2} \right)} \end{array} \right. \quad (2.3.7)$$

Looking at the summary formulas, it can be noticed that inside the STR compensation does not appear the terms M and R_L . Therefore, for a chosen value of C_1^{STR} the resonant condition does not change with M and R_L . Thus, this type of compensation results particularly suitable for dynamic application with respect to the parallel configuration.

2.4 Hybrid topologies

Besides the basic compensation topologies previously discussed, there are other types of compensation that brings together the series and parallel compensation characteristics, as reported in fig. 2.5

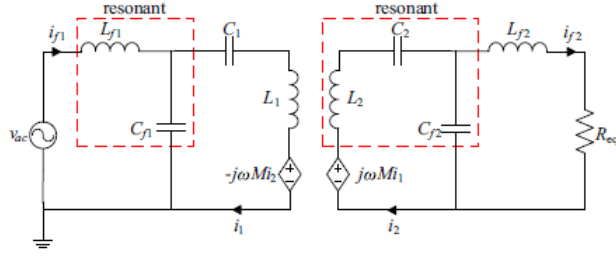


Figure 2.5: Hibrid compensation topologies [3]

As shown in fig. 2.5 the inductance L_{f1} resonate with the capacitors C_{f1} keeping i_1 constant and the induced voltage $j\omega M i_1$ will be constant as well. The resonant condition on the receiver side aims to make the resonant frequency independent from the load condition and the coupling factor. Moreover, the output current is constant which is a hoped condition for battery charging. The negative sides of this compensation are: the use of further inductances L_{f1} and L_{f2} to mitigate the current peaks and the additional use of capacitors. This imply costs increase, less reliability, more volumes and more complex connections.

2.5 Efficiency

An important parameter of the IPT system is the efficiency. Between the different stages of the energy transformation, there are many types of losses, such as: electronic converter losses, winding joule losses, iron losses, conductive losses in the near material (shield), capacitors losses, ext. For these reasons, an accurate estimation of all of these losses is very complex. Nevertheless, a general efficiency expression can be derived from from the circuit model:

$$\eta = \frac{R_L I_L^2}{R_1 I_{L1}^2 + R_2 I_{L2}^2 + R_L I_L^2} \quad (2.5.1)$$

A better efficiency expression can be found fixing a compensation topology and explicating the current expression:

- Series compensation

$$\hat{I}_1 = \hat{I}_1 \quad (2.5.2)$$

$$\hat{I}_2 = \frac{j\omega M I_1}{\left(R_2 + R_L + j \left(\omega L_2 - \frac{1}{\omega C_2} \right) \right)} \hat{I}_L = \hat{I}_2 \quad (2.5.3)$$

$$\hat{I}_L = \hat{I}_2 \quad (2.5.4)$$

- Parallel compensation

$$\hat{I}_{L1} = \hat{I}_1 - j\omega C_1 \hat{V}_1 \quad (2.5.5)$$

$$\hat{I}_2 = \frac{j\omega(1 + j\omega R_L C_2)}{R_L + (R_2 + j\omega L_2)(1 + j\omega R_L C_2)} \hat{I}_1 \quad (2.5.6)$$

$$\hat{I}_L = \frac{1}{1 + j\omega R_L C_2} \hat{I}_2 \quad (2.5.7)$$

Substituting these current in 2.5.1 they can be found two efficiency expressions depending from the compensation topology:

$$\eta^{STR,PTSR} = \frac{R_L}{(R_L + R_2) \left(1 + R_1 \frac{R_2 + R_L}{\omega_0^2 M^2} \right)} \quad (2.5.8)$$

$$\eta^{STR,PTSR} = \frac{R_L}{R_L + R_2 + \frac{R_2 R_L^2}{\omega_0^2 L_2^2} + \frac{R_1 R_2^2}{\omega_0^2 M^2} + \frac{R_1 R_2^2}{M^2}} \quad (2.5.9)$$

These two expressions can be linked with the coupling factor k . In fact the coupling factor is:

$$k = \frac{M}{\sqrt{L_1 L_2}} \quad (2.5.10)$$

Consequently, the M can be written as:

$$M = k^2 L_1 L_2 \quad (2.5.11)$$

if k increases the value of M increase as well. Therefore, the denominator decreases and the system efficiency increases.

2.6 Conclusion

In this chapter the main IPT characteristics have been discussed starting from the basic physical laws that explain hoe the system works. A general view of the system components have been discussed exploiting a block diagram Secondly, the basic equations have been translated in an equivalent circuit. This latter has allowed to define the basic IPT parameters After, the different types of compensation have been showed, explaining pros and cons of every topology and giving a quick look to the existent hybrid topologies as well. Finally, the system efficiency has been introduced. At this point, it is important to look at the actual geometries proposed by the years by research community so far.

Chapter 3

State of the art

3.1 State of the art

In this chapter a resume of the most important papers used as reference for this thesis is made. In these years many kind of topologies have been proposed, but only some of them can have an actual application. In fact, some of the available geometry in literature have better performances than others in terms of: general performance, feasibility and cost effectiveness. So, this type of topologies have been searched. The selected coils can be classified in two macro-groups: polarized and non-polarized. The first coil type, circular and rectangular, simply creates closed flux line around the coil wire. The second coil type creates two magnetic poles and the flux lines goes from one pole to the other, creating a pipe line. The DD and DDQ coil types, that will be showed in the next chapter, are polarized type coils.

This chapter is splitted in two sections: the first one collect all the studies that propose the circular geometry. The second section expose the rectangular type form and its derivatives.

3.2 Circular geometry

In this section will be described two interesting paper that have carried out a study on the circular coil type. This type of pad is debated a part, because it is one of a kind.

Paper one

In [4] is presented a circular pad for IPT lumped structures. The work is focused on a 2 to 5 kW system with an air-gap of 200 mm. At the beginning, a small-scale pad layout has been built-up to validate the output simulation. For this first pad are used: the available ferrite bars, nominal wire current and experience. After, an optimization process is carried out starting from the basic pad used to validate the simulation results, showed in fig. 3.1. The optimization process starts fixing the variables reported in fig. 3.1, where: the component dimensions are given by the available material; the power supply is assumed: $I_1=12$ A, $f=50$ Hz; the number of turns is equal to 12, because is a good compromise between: coupled power, power losses, self-inductance and ferrite flux density. Four different changes are carried out: spread the coil, change the coil center diameter, or to maintain the same center diameter while moving the ferrites radially inward or outward.

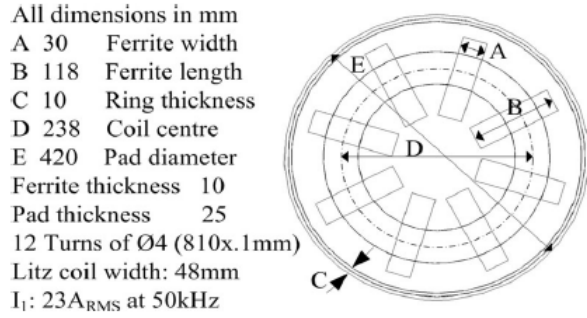


Figure 3.1: Basic coil layout [4]

Changing the pad layout without adding extra ferrite bars

The maximum output power is reached at the 90% of the original base pad, which is approximately the 40% of the ferrite length. Executing the other parameters variation it can be noticed that the performance are determined by the relative position between the coil and the ferrite bars. Referring to fig. 3.2

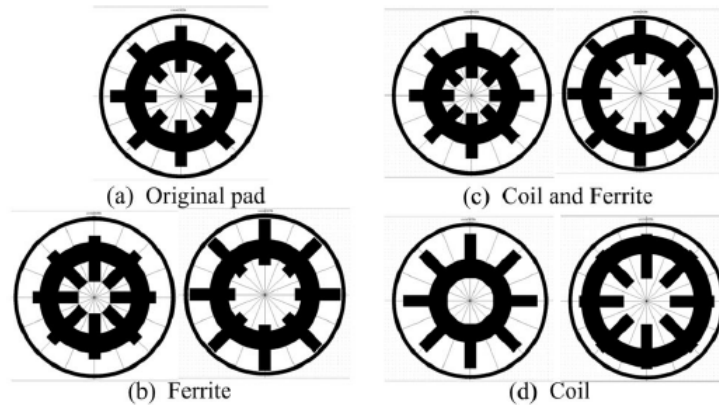


Figure 3.2: Various configurations of pad layout used in the optimization process [4]

the maximum transferred power is achieved moving outward of 4 mm the coil and an moving in the ferrites. Combining these two condition the optimum is achieved if the ferrites are offset towards the center forming a ferrite central diameter of 230 mm.

Improving coupling by adding ferrite

In this second stage, it is checked what vary changing the ferrite bars characteristics: length, number of bars, thickness and width. Resulting that the bars length has the bigger impact on the transferred power, while the thickness does not influence it.

Relating power and pad size

The basic 420 mm pad size is not able to achieve the minimum power requested. So, keeping the layout factor previously founded, different diameters for various air-gap have been tested as reported in fig. 3.3

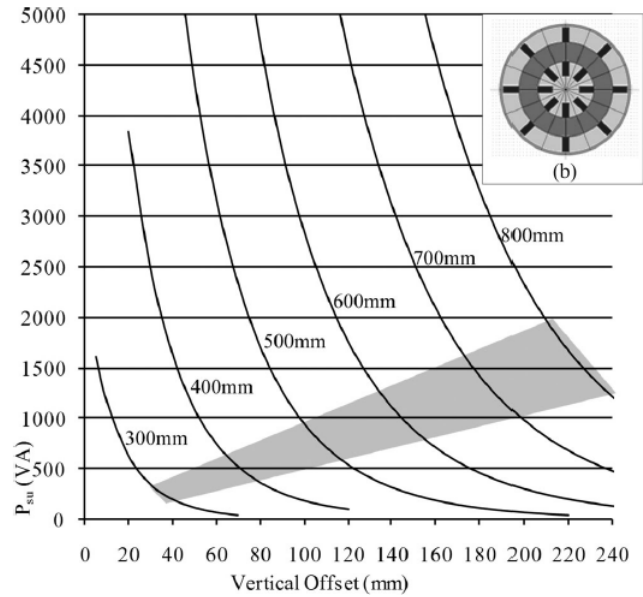


Figure 3.3: Power outputs for different air-gap and coil diameter [4]

The pad diameter that ensure a 2 kW of power transferred for 200 mm of air-gap is 800 mm, but the chassis vehicle area and the cost-effectiveness limitations bound this diameter. So, a 600 mm pad diameter was chosen carrying out an optimization process to achieve the wanted power transferred.

Optimization of a 5 kW 600 mm pad with a 150 mm of air-gap

In this section, the study propose a pad layout in order to provide 5 kW at 150 mm of air-gap. The basic pad characteristics are: number of turns equal to 18, ferrite bars as long as possible and a coil 57% of pad diameter. With this configuration, it is not able to transfer 2 kW of power with 200 mm of air-gap at 100 mm of displacement. So, a further ferrite configuration is needed. Others five ferrite configuration are analyzed trying to find a good compromise between the transferred power, field shape, actual feasibility of the structure. The final configuration that combines all these characteristics is reported in fig. 3.4.

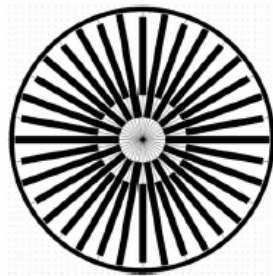


Figure 3.4: Final layout [4]

Paper two

In [5] a ferrite-less circular coil is proposed, called circular non-ferrite pad (CNFP). This pad is characterized by the ability to control the leakage flux in order to reduce the electromagnetic field outside the charging space. It is able to do that using an auxiliary coil, based on the Helmholtz coil theory. This system of coils allows to reach a better cost-effectiveness respect to a classic ferrite-type coil. It is composed by two coils, the transmitter and its auxiliary, with a series-opposing configuration. This configuration permits to minimize the stray field under the pad and outside the charging area. The coil layout is depicted in fig. 3.5.

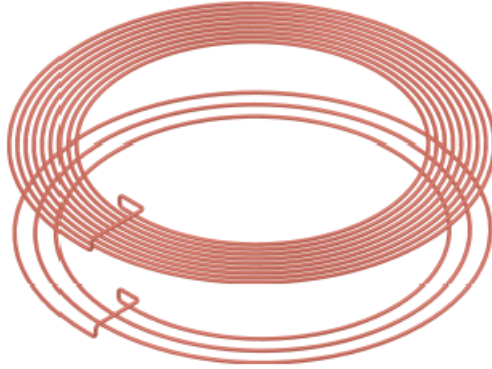


Figure 3.5: Circular non-ferrite pad layout [5]

This structure is based on the Helmholtz coil theory. In this case the aim is not a uniform field between the coil, but shaping the field in order to minimize it underneath and outside the coil region. In order to achieve that, a proper N_1/N_c turns ratio and h distance between the coils have to be found.

Thanks to the Biot-Savart law the z -axis field can be calculated as the sum of the two B_z generated by the coils.

$$B_z = B_1 + B_c = \frac{\mu r^2}{2} \left[\frac{N_1 I_1}{(r_1^2 + z^2)^{\frac{3}{2}}} - \frac{N_c I_2}{[r_c^2 + (z+h)^2]^{\frac{3}{2}}} \right] \quad (3.2.1)$$

In figure 3.6 it can be seen that using a proper N_1/N_c ratio for a fixed h distance different field shapes can be obtained.

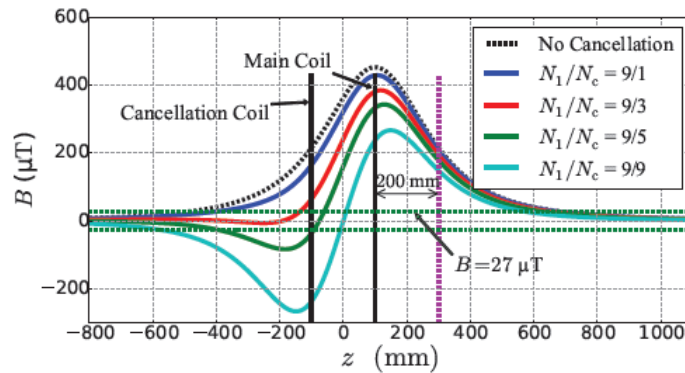


Figure 3.6: Ferrite-less coil field shapes changing the number of turn ratio [5]

To find the optimal N_1/N_2 ratio, the ratio between the area under B_z curve on the top of the pad and the area under the B_z curve under the bottom side of the pad is used. For $N_1/N_2=3$ the optimal ratio is achieved.

A laboratory prototype is proposed in table 3.1 and it is used to validate the experimental results.

Parameters	Description	Value
L_{eq}	CNFP Inductance	51.51 μ H
R_{loss}	Pad resistance at 38.4 kHz	81.6 m Ω
I_1	Primary current	20 A
OD_1	Main coil outer diameter	500mm
OD_C	Cancellation coil outer diameter	500mm
ID_1	Main coil inner diameter	357.2mm
ID_C	Cancellation coil inner diameter	357.2mm
C_W	Copper winding width	71.4mm
h	Main cancellation coil distance	100mm
N_1	Main coil number of turns	9
N_C	Cancellation coil number of turns	3

Table 3.1: coil parameters [5]

Using the coil set-up reported in table 3.1 and inserting a ferrite type receiver of the same diameter others interesting results have been found.

First, increasing the auxiliary coil diameter from 500 mm to 750 mm the coupling factor slightly decrease. Another surprising result is that increase the auxiliary coil diameter the leakage flux decrease. A good compromise between the previous results can be a diameter between: 655 to 670 mm. The h distance influences several important parameters. The coupling factor increases significantly with increasing h , but the uncompensated apparent power at the secondary coil tends to increase. So, it is important to choose an optimal h distance. For this study $h = 100$ mm.

3.3 Rectangular coil types

In this section are gathered together all the papers that treat rectangular coil type and its derivatives.

Paper one

This paper [6] proposes a rectangular coil type for public transportation. It was crated and optimized to operate according to characteristics reported in table 3.2.

Parameters	Variable	Value
Output power	P_2	50 kW
Transmitter side DC Voltage	$U_{1,dc}$	0-800 V
Receiver side DC Voltage	$U_{2,dc}$	0-800 V
Battery Voltage	U_{batt}	500-700 V
Air-gap	z	100-200mm
Positing Tolerance	$\Delta x,y$	± 150 mm
Transmission frequency	f_0	85 kHz

Table 3.2: System characteristics [6]

The proposed coil has the follow geometry reported in fig. 3.7:

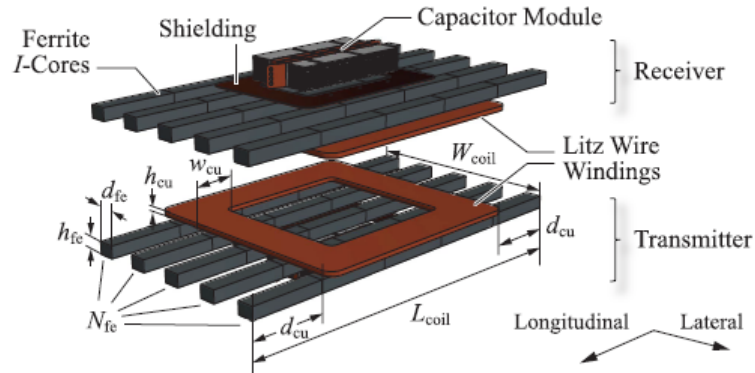


Figure 3.7: Rectangular coil proposed [6]

A rectangular coil type is chosen to better match the vehicle geometry and the I-core bars type are added to improve the magnetic coupling without adding too much weight.

A 3D FEM model is made considering a solid copper winding with a constant current density. The self-inductances (L_1 and L_2), the mutual inductance M and the coupling factor k are calculated by the magnetic energy calculation with this simplified model. The simulation results are validated by measured parameters on the prototype. The difference between the simulated a measured values is under the 10%.

An optimization process is carried out to chose the best coil geometry, taking into account different Pareto front optimums taken from three different optimizations:

- efficiency-power density-coupling factor
- efficiency-gravimetric power density-number of bars
- power losses-strayfield-coil area

where:

the gravimetric power density is $\gamma = P_2/M_{coil}$; the power density is defined as $\alpha = P_2/A_{coil}$.

Matching all these data the coil in table 3.3 is proposed:

Variable	Value
W_{coil} (mm)	380
L_{coil} (mm)	630
d_{cu} (mm)	125
w_{cu} (mm)	67.5
N_{fe}	5
N_1, N_2	9.5
C_1, C_2 (nF)	54.1
Litz wire	2500x0.1 mm
Ferrite cores	I-126/20, k2004
Resonant caps	CSP 120-200
Shielding	OFC, 2 mm thick

Table 3.3: System characteristics [6] (Turns number "9.5" means that connections are at opposite sides of winding)

Paper two This study [7] have carried out a comparison between rectangular and double-D coils for a 50kW/85kHz IPT system.

The double-D coil is a polarized coil type derived from a rectangular coil type. It is generally realized winding a wire in two opposite way from one side to the other. In this way two magnetic poles are created, for this the reason it is a polarized coil type. The flux line is guided from the north to the south pole, as depicted in fig. 3.8

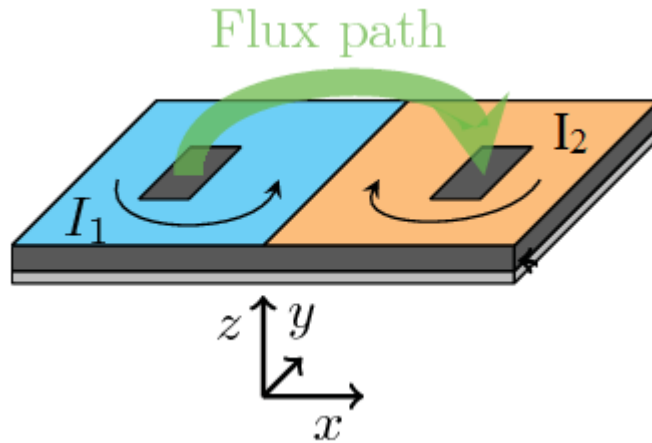


Figure 3.8: DD flux path [8]

The two coil geometries are reported in fig. 3.9

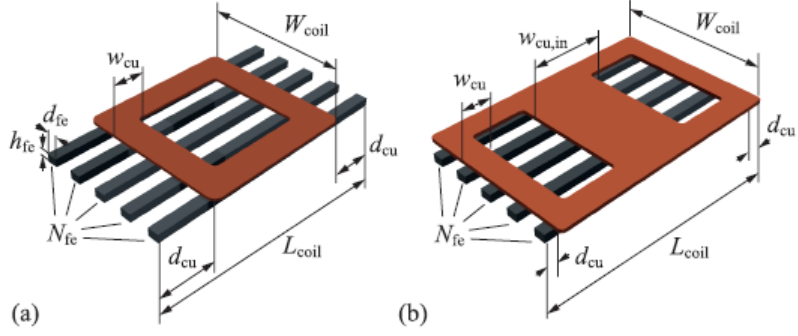


Figure 3.9: Proposed rectangular and DD coils [7]

The study analyses some performance factors, such as: efficiency, power density, and stray field. In order to compare these two coils a multi-objective analysis is carried out, analyzing the degree of freedom reported in table 3.4

Variable	Min (mm)	Max (mm)	step (mm)
W_{coil} (mm)	300	700	50
L_{coil} (mm)	300	700	50
d_{cu} (mm)	50	150	25
w_{cu} (mm)	50	150	25
$w_{cu,in}$	50	150	25
N_{fe}	3	7	2

Table 3.4: Design parameters for the optimization [7]

The comparison results show some main differences between the two coils:

- The magnetic coupling is better for rectangular coil
- For a given efficiency the double-D coil is heavier than the rectangular coil
- The core flux density of double-D is higher than the rectangular one. For this reason, it needs more ferrite bars to avoid saturation
- The power losses are 50% more for the double-D due to the flux density
- The double-D coil has higher total losses than rectangular one
- The double-D coil has a better stray field behavior: it has less stray-field outside the coil area because the flux lines are well shaped.

using the Pareto front optimums of the optimization process, two coil prototypes are proposed in table 3.5.

Variable	Rectangular	Double-D		
W_{coil} (mm)	380	380		
L_{coil} (mm)	630	360	Litz wire	2500x0.1 mm
d_{cu} (mm)	125	18	Ferrite cores	I-126/20, k2004
w_{cu} (mm)	67.5	56	Resonant caps	CSP 120-200
$w_{cu,in}$	n/a	90	Shielding	OFC, 2 mm thick
N_{fe}	5	5		
N_1, N_2	9.5	6.5		

Table 3.5: Design parameters of the realized prototype [7]

Paper three

This paper [9] shows a new topology based on the double-D pad, composed of two rectangular coils partially overlapped. Polarized pad is interesting because has a better reaction to misalignment and lower stray field in the outer coil region. This new coil topology is created keeping as reference the double-D geometry and shifting toward each other each "D coil". This set-up allows to decoupled each "D coil" from the other one. Therefore, the obtained coil can be driven with a particular phase and magnitude in each side of the coil. This technique opens to the possibility to coupling it with different types of receiver.

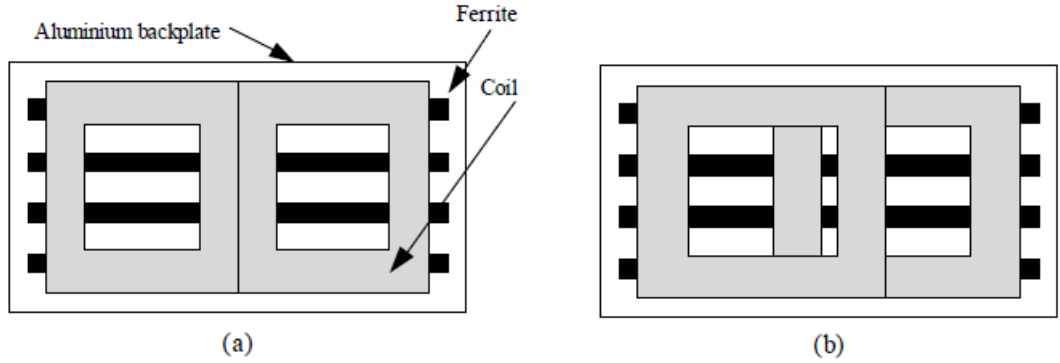


Figure 3.10: a) double-D b) overlapped double-D [9]

This study investigates three different coils with the same dimensions, but changing the number of ferrite bars (6,8,10). For each configuration is searched the condition of zero mutual inductance between the two "D" of the double-D coil. The geometry coil characteristics are reported in table 3.6 and 3.7.

Attribute	Value
Winding Width	80 mm
Ferrite spacing	32 mm
Ferrite width	28 mm
Y coil spacing	50 mm
Y padding	46 mm
Cover thickness	6 mm
Coil height	16 mm
Spacer thickness	6 mm
Aluminum thickness	4 mm

Table 3.6: Pad dimensions [9]

Attribute Value			
Ferrites	6	8	10
Ferrites length	558	744	930
Overlap	156	74	39
X coil spacing	10	-83	-174
X padding	10	10	110

Table 3.7: Pad dimensions [9]

The advantages of a overlapped double-D transmitter is that each side can be driven independently from the other one. If the currents are driven equal in magnitude and 180° out of phase, a pulsating field can be created. Instead, if it is driven by two same magnitude currents and 90° out of phase, it will be generated a rotating field. Moreover, one coil can be turned off if there is no need of it.

The study uses a double-D quadrature coil as receiver. This is a type of coil derived from the double-D coil. Basically adding a third placed in the middle with respect to the two double-D coil, depicted in fig. 3.11. This set-up guarantees a good coupling even when the double-D coil is completely displaced with respect to the transmitter, because the quadrature coil will be centered.

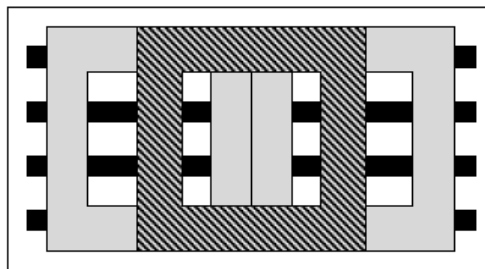


Figure 3.11: DDQ design [9]

In fig. 3.12, a 8 bars ferrite type transmitter is driven using a (180°) and a pulsating (90°) technique. The current magnitude is 23A at 20kHz. A normal double-D coil is used as transmitter in order to have a therm of comparison. The receiver is a DDQ coil at a distance of 200 mm.

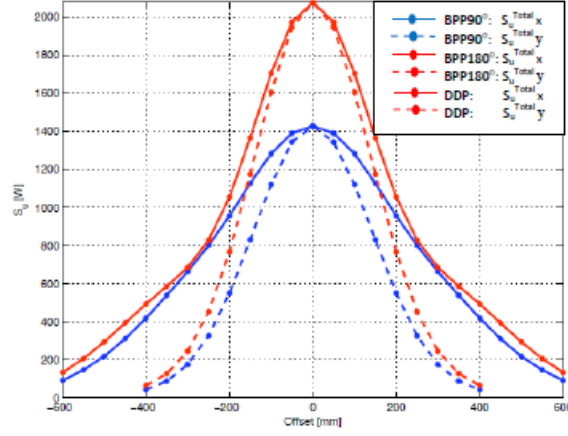


Figure 3.12: Power transferred with two phase and in phase current drive and using a DD receiver [9]

As can be seen the maximum power transferred is for bipolar driven coil. It has a better misalignment behavior as well.

The power transferred is analyzed for different number of bars. The result is that the power transferred increase with the numbers of bars, but the best result is between six and eight bars.

Paper four This study [10] considers two types of geometries: rectangular and double-D. Its aim is to achieve the maximum coupling coefficient and the maximum efficiency for the minimum size of the secondary coil. The coils proposed are reported in fig. 3.13

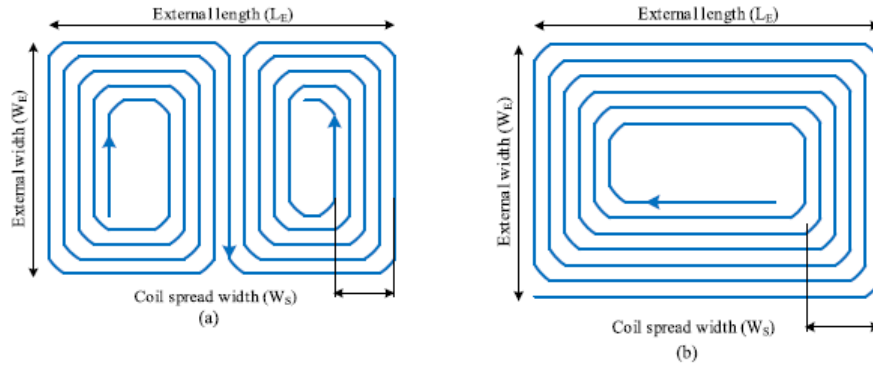


Figure 3.13: a) DD coil b) unipolar coil [10]

The secondary coil external dimension (length and width) are fixed. While the length, the with and the coil spread of the primary coil are optimized.

In order to fix others coupling related factors, a coils optimization is carried out. A unipolar coil, with the fixed parameters reported in table 3.8, is used to fix the coil related parameters.

Unipolar coil size Values (mm)		
Secondary coil	LE_{sec}	250
	WE_{sec}	250
	WS_{sec}	50
Primary coil	LE_{pri}	450
	WE_{pri}	450
	WS_{pri}	240
	Air-gap	150
	Vehicle chassis size	1200x1200
Coil	Coil layer thickness	1 to 15
	Space between turns	0.1 to 2
	Ferrite material permeability	1 to 3000
Shielding	Primary shielding size	0x0 to 1000x1000
	Secondary shielding size	0x0 to 1000x1000
	Distance between the chassis and the back plate	0 to 100
	Thickness	1 to 5

Table 3.8: Simulation parameters [10]

Ferrite bars

First, a comparison analysis is carried out to fix the number of ferrite bars. The coupling factor is rise increasing the number of bars, but with a limited slope from 24 to 36 bars. A magnetic plate is selected for simplification. For the unipolar coil the same the coil dimension is chosen. For the double-D the configuration with the maximum k .

Coil

The simulation results indicate that the higher the coil thickness is the lower is the coupling factor. For this reason, a wire diameter of 4 mm is chosen.

Shielding and vehicle chassis

The vehicle chassis is simulated using a metal plate of 1200x1200 mm.

Secondly, the simulation results show that increasing the distance between the vehicle chassis and the shield D_s , the k value goes down. For practical consideration is chosen $D_s=10$ mm.

The aluminum shield dimensions are the same as the coil.

The simulation results highlight the following factors:

- The double-D coil needs a 1.6 length-width ratio with respect to the rectangular coil
- The double-D has a better efficiency and value of k , but it needs larger primary coil dimensions
- The double-D seems to have a better behavior with respect to the misalignment, even if it needs a larger transmitter dimension with respect of the rectangular geometry
- A re-designed coil is made to obtain better performances for misalignment conditions, in particular for the maximum operating capability condition (MOC). The MOC is defined to output the maximum power at misalignment distances of: 75 mm (x direction) and 100 mm (y direction)
- The coil optimized for the MOC case improve its performance to misalignment, but is worse for the no-misalignment case

- The new coil needs a larger dimensions. For instance, for a 250x250 mm secondary coil, the previous primary coil is 450x450 mm, while the MOC coil 620x650 mm

Paper five This paper [11] wants to realize an on road IPT system using a DD geometry as transmitter and DDQ as receiver. The coils geometries are depicted in fig. 3.14:

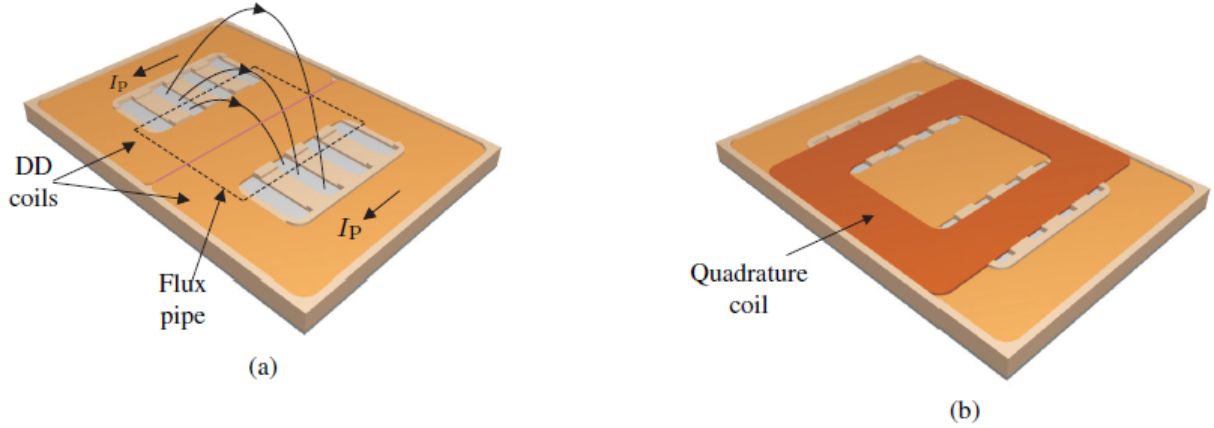


Figure 3.14: a) DD geometry b) DDQ geometry [11]

The DD and DDQ coil types have been chosen because they have a better behavior to misalignment. In particular they allow to avoid a zero power transferred. This is due to the quadrature coil of the DDQ coil used as receiver. In fact, it starts to increase its power when the DD power starts to fall down with misalignment. It can be seen in fig.3.15:

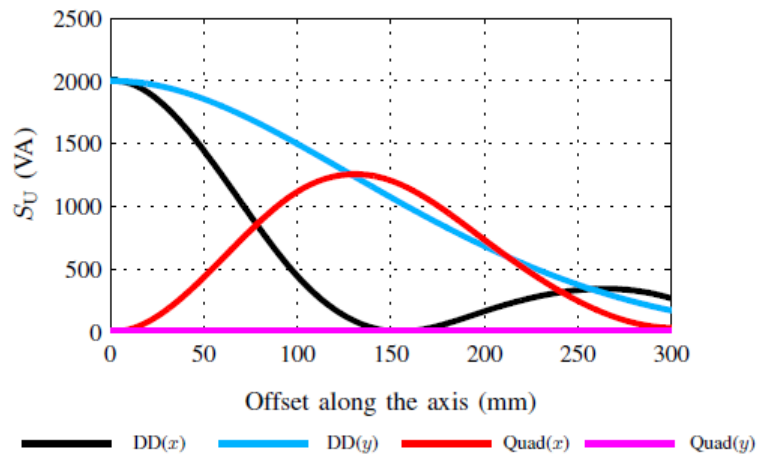


Figure 3.15: Apparent power profile for DD-DDQ system [11]

A series of pad sizes are analyzed in order to transfer 10 kW independently if the vehicle is a sedan or SUV.

Primary pads (m)	Secondary pads (mm)
Pri 255x280	Sec 280x352
Pri 395x390	Sec 370x410
Pri 510x475	Sec 465x495
Pri 630x620	Sec 560x580
Pri 745x705	Sec 745x690
Pri 745x825	Sec 835x800
Pri 865x910	Sec 930x885
Pri 980x995	Sec 1025x1030

Table 3.9: Proposed pad size [11]

An analytic model is proposed, based on a bell-distribution, in order to find a proper primary coil distance. This distance have to unsure no magnetic coupling between two adjacent primary coils. Moreover, it have to allow a as possible as constant transferred power when the vehicle travel along the road. The optimal distance between the two coils centers is 525 mm. This coils distribution gives the current vehicle profile reported in fig 3.16

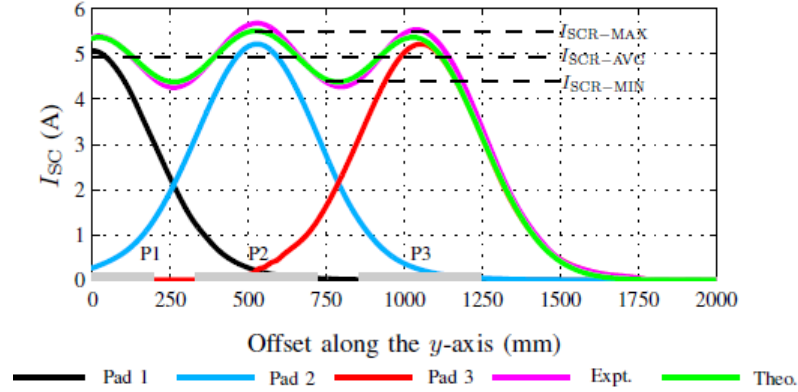


Figure 3.16: Current induced profile [11]

An optimization process is carried out to find the coil sizes and the number of coils per kilometer. The best configuration results 865x910 (mm) with a distance between the coils of 1327 (mm).

3.4 Considerations

The papers analyzed in this chapter give many informations on each coil performance. Looking at each coil topologies, the unipolar coils certainly have some pros, such as: guarantee high coupling factor, lightness, easy to realize. On the other hand, the main cons are lower coupling factors with respect to misalignment and high stray-field.

The polarized geometries basically have a better reaction to misalignment and minor stray-field. This because of their better field shape. They offer the possibility to being decoupled and driven with different techniques. Therefore, they offers the possibility to interoperate better with other type of receives. As cons they are heavy and have a more complex winding structure.

However, these papers, analyze one coil at a time or at most are compared two coil in the

same paper. At this point, it can be useful to compare all these geometries with some well defined evaluation criteria. In order to verify if the known results are real, taking into account all the other coils.

Chapter 4

Comparison

4.1 Introduction

In this chapter will be discussed the evaluation criteria used to initialize the comparison and the theory used to calculate the parameter. The thesis aim is to understand each coil pros and cons comparing each of them under the same conditions. The chosen evaluation criteria are a trade-off between the previous analyzed papers and the last automotive standards released.

4.2 Coil layout criteria

Three coil characteristics are fixed:

- **Coil area** (A_{ref}): this is the effective area of the coil that link the magnetic flux
- **Number of turns** N_t : this parameter influences the self and the mutual inductance of the coils
- **wire diameter** D_0 : this parameter influences the coil winding spread

Coil area

The first comparison criteria that has been fixed is the external coil area, as depicted in 4.1

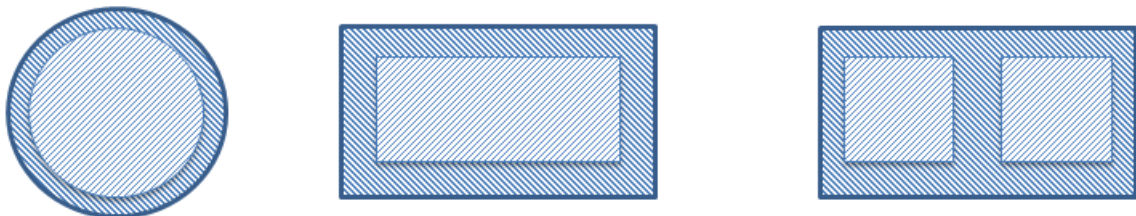


Figure 4.1: Coils area: a) circular b) rectangular c) double-D

the external coil area is the sum of the internal light blue and deep blue area.

Maintaining the coil area constant allows to:

- Have the same area that links the same flux density. It allows to compare the obtained k values and flux density B.
- To compare and highlight each coil behavior versus the displacement. If a coil would be bigger than another one, it surely would have a better behavior to misalignment with respect to the small one.

Once the coil area is fixed, the actual coil dimensions (each side dimension) have to be chosen. In order to decide the dimensions, the reference released by the SAE International: a global association that releases norms in aerospace, automotive and commercial-vehicle fields. The SAE J2354 [12] is the thesis reference. This reference establishes and defines the acceptable criteria for interoperability, electromagnetic compatibility, EMF, minimum performance, safety and testing for wireless charging of light duty electric and plug-in electric vehicles.

In the SAE J2954 standard some WPT power classes are defined with a minimum target of efficiency reported in table 4.1:

WPT Power Class)				
	WPT1	WPT2	WPT3	WPT4
Maximum input Volt Amps	3.7 kVA	7.7 kVA	11.1 kVA	22 kVA
Minimum target efficiency at nominal x,y misalignment	<85%	<85%	<85%	TBD
Minimum target efficiency at offset position	<85%	<85%	<85%	TBD

Table 4.1: WPT power classes according to SAE J2154 [12]

the power classes WPT1 and WPT2 are defined to match the power requirements specified in the previous standard. The power class WPT3 is defined provisionally and WPT4 is still in a definition status. As can be seen in fig. 4.1, for each class there is a minimum system efficiency for the no-misalignment case and the offset condition. The main aim of the standard is to guarantee the interoperability between different power classes, for instance: a transmitter coil of WPT1 power class has to be able to operate with a receiver of WPT2 power class, ensuring at least the reported efficiency.

The J2954 proposes in its appendix the transmitter coil dimension. This one can operate with three different receivers belonging to the WPT1 class for all the z-classes (they will be defined later). In fig. 4.2 are reported the coil dimensions:

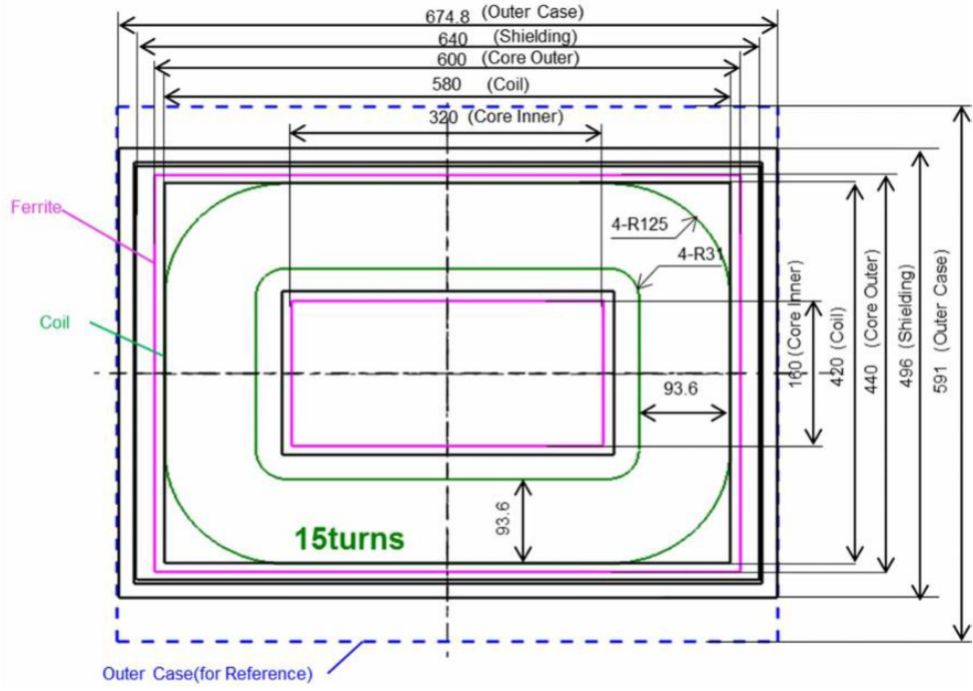


Figure 4.2: Reference coil dimensions [12]

The coil area (A_{ref}), corresponding with these dimensions, has been chosen as reference for the coils comparison. For the rectangular coil the dimension are simply equal. For the circular geometry, an equivalent radius r_{eq} can be defined

$$r_{eq} = \sqrt{\frac{1}{\pi} A_{ref}} \quad (4.2.1)$$

For the polarized coil, the outer area is imposed equal to the rectangular one. The chosen area is maintained equal for both receiver and transmitter in order to avoid differences in the comparison.

Therefore, as reported in fig. 4.2 the coil reference dimensions, for both receiver and transmitter, are: 580x440 mm.

Wires diameter D_0

The wire diameter is $D_0 = 5mm$ for all coils. Because the order of the current magnitude is about 10 A. So, this diameter is largely used to have a suitable current density.

Number of turns

The number of turns is fixed to $N_t = 15$, as depicted in fig. 4.2. The equal number of N_t is used for the following reasons:

- The number of turns influences the self-inductance of both transmitter and receiver, because it is proportional to N_t^2 . At the same time it is linked with the mutual inductance between the transmitter and the receiver by the product of their N_t . Both these factors compare in the coupling factor expression. Therefore, to fairly compare the k values is useful take N_t constant. Moreover, keeping constant N_t every coil will have the same ampere-turn ratio. This allows to compare the magnetic flux density B.
- Keeping constant the wire diameter D_0 allows to have same coil winding spread.

These IPT parameters have been chosen because they can give useful information about the coil behavior without define boundary condition, such as: the compensation topology, the load type and the used electronic converters to drive the coils. This allows to make the comparison as general as possible.

4.3 Evaluation parameters

The two evaluation parameters are:

- The coupling coefficient k
- The coil magnetic flux density \mathbf{B}

4.3.1 Coupling coefficient k

The coupling coefficient is defined as:

$$k = \frac{M}{\sqrt{L_t L_r}} \quad (4.3.1)$$

where: L_t and L_r are respectively the transmitter and receiver self-inductance and M is the mutual inductance between them.

k is an important parameter for the IPT system, because it contains many information on the system behavior. First of all, it describes the ratio between the linked flux with respect to the flux generated by the transmitter. For this reason it gives indirectly an information of the power that can be transferred from the transmitter to the receiver. This one is linked with the system efficiency as well.

The value of k is directly proportional to the mutual inductance M and inversely proportional to the L_1 and L_2 square root product. So, to compute it, these inductances must be calculated.

Inductance expression [13]

The inductance calculation used in this thesis is based on the vector potential calculation. Therefore, it is first necessary to introduce it.

In electrostatics the divergence of the electrical field is zero:

$$\Delta \times \vec{E} = 0 \quad (4.3.2)$$

consequently it is possible to represent the electrical field, up to a constant, by a scalar potential:

$$\vec{E}_0 = -\Delta V \quad (4.3.3)$$

In the same way for magnetoquasistatic field it can be write:

$$\Delta \cdot (\vec{B}) = \Delta \cdot (\mu_0 \vec{H}) = 0 \quad (4.3.4)$$

therefore, the B field can be expressed by the vector potential A , as:

$$\vec{B} = \mu_0 \vec{H} = \Delta \times \vec{A} \quad (4.3.5)$$

The magnetic flux λ through a surface can be expressed by the integral of B field on the surface:

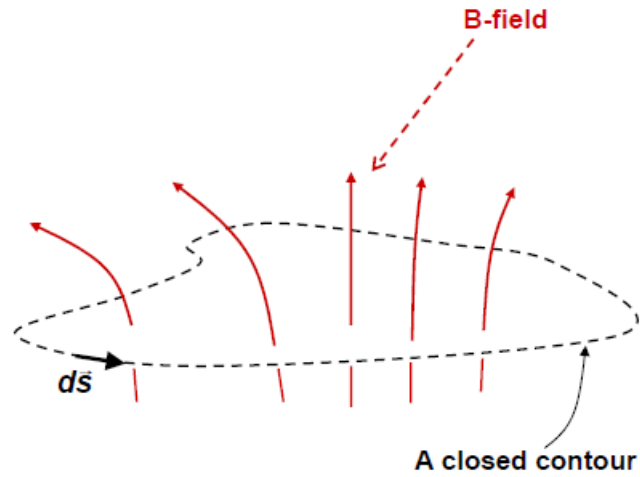


Figure 4.3: Magnetic flux through a surface [13]

$$\lambda = \iint \vec{B} \cdot d\vec{a} = \mu_0 \iint \vec{H} \cdot d\vec{a} \quad (4.3.6)$$

using the previous relation

$$\vec{B} = \mu_0 \vec{H} = \Delta \times \vec{A} \quad (4.3.7)$$

it can be get:

$$\lambda = \iint \vec{B} \cdot d\vec{a} = \iint (\Delta \times \vec{A}) \cdot d\vec{a} \quad (4.3.8)$$

and, exploiting the Stokes relation:

$$\lambda = \oint \vec{A} \cdot d\vec{l} \quad (4.3.9)$$

the magnetic flux through a surface can be expressed by the line-integral of the vector potential along a closed contour bounding that surface.

Inductance

The magnetic flux enclosed by current carrying conductors is directly proportional to the current carried by the conductors:

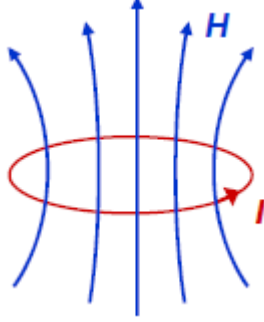


Figure 4.4: Magnetic flux enclosed a closed conductor [13]

the constant proportion is defined by the ratio between flux λ and the current I :

$$\lambda = LI \quad (4.3.10)$$

$$L = \frac{\lambda}{I} \quad (4.3.11)$$

The magnetic energy stored by an inductor can be expressed by the follow relation:

$$W = \frac{1}{2}LI^2 \quad (4.3.12)$$

in a generic circuit the stored energy is given by the product between a current and a flux:

$$W = \frac{1}{2}I\lambda \quad (4.3.13)$$

using the previous relation found in 4.3.9:

$$W = \frac{1}{2}I \oint \vec{A} \cdot d\vec{l} \quad (4.3.14)$$

it can be computed the magnetic energy \mathbf{W} through the vector potential. Finally, the self inductance is:

$$L = \frac{2W}{I^2} \quad (4.3.15)$$

To obtain the mutual inductance, if there is current-carrying with a current I_1 that enclose a magnetic flux in a second circuit λ_{12} , the mutual inductance is:

$$\lambda_{12} = MI_1 \quad (4.3.16)$$

$$M = \frac{\lambda_{12}}{I_1} \quad (4.3.17)$$

The value of \mathbf{M} can be obtained with the same procedure followed for self-inductance coefficient L .

4.4 Coupling coefficient of IPT

Each inductance term has been numerical calculated using dedicated functions contained in DualLab, a Matlab suite developed by the Prof. Fabio Freschi. The inductance calculation aims to evaluate an equivalent transmitter and receiver self-inductance respectively L_t and L_r in order to use it in the k calculation. The calculation of the stored magnetic energy is made approximate a massive coil to a N-turns wire coil, clearly maintaining the same coil width. The inductance calculation accuracy is verified by comparing the results computed with this method with the magnetic parameters declared in some studies found in literature respecting the same coil dimensions.

In the following sections the procedure to evaluate the k related parameters will be discussed. It includes the two self-inductance calculation and the mutual inductance as well.

4.4.1 Unipolar coils

The two unipolar coils proposed are:

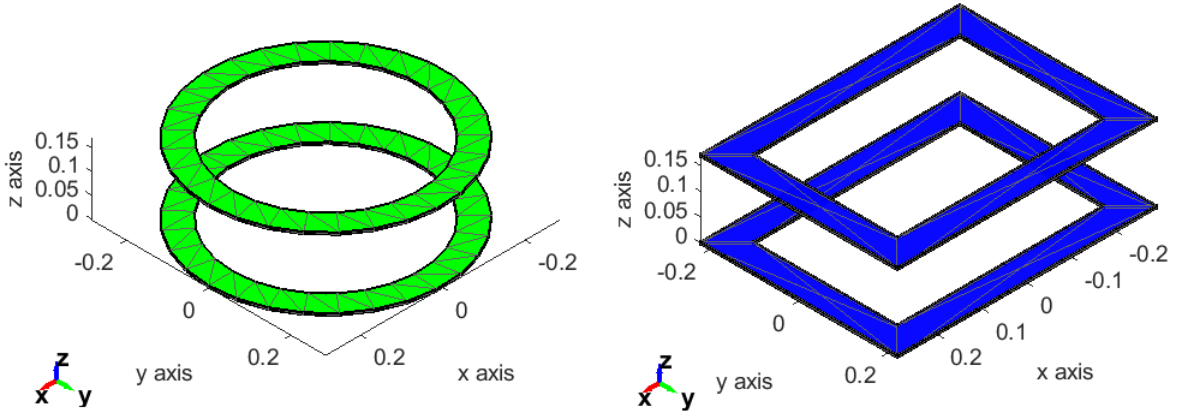


Figure 4.5: a) Circular coil geometry b) Rectangular coil geometry

For a system formed by two unipolar coils (receiver and transmitter) the following equation can be written:

$$\begin{cases} \hat{V}_1 = j\omega(L_{11}\hat{I}_1 + L_{12}\hat{I}_2) \\ \hat{V}_2 = j\omega(L_{21}\hat{I}_1 + L_{22}\hat{I}_2) \end{cases} \quad (4.4.1)$$

L_{11} and L_{22} are respectively to the transmitter and receiver self-inductance, for this reason they can be posed $L_{11} = L_t$ and $L_{22} = L_r$. For the system symmetry L_{12} is equal to L_{21} , so both can be put equal to mutual transmitter-receiver inductance M : $L_{12} = L_{21} = M$.

Therefore, it can be written:

$$\begin{cases} \hat{V}_t = j\omega(L_t\hat{I}_1 + M\hat{I}_2) \\ \hat{V}_r = j\omega(M\hat{I}_1 + L_r\hat{I}_2) \end{cases} \quad (4.4.2)$$

In order to calculate the coupling coefficient k , the following procedure is carried out:

- The coil structure is drawn using the customized Matlab function *cretcoil3d*.
- The related vector potential is calculated exploiting the custom function *coilVectorPotential3d*
- The magnetic energies related with every inductance are computed
- Each inductance term is computed
- The coupling factor k is calculated

4.4.2 Polarized coils

Double-D and Double-D overlapped

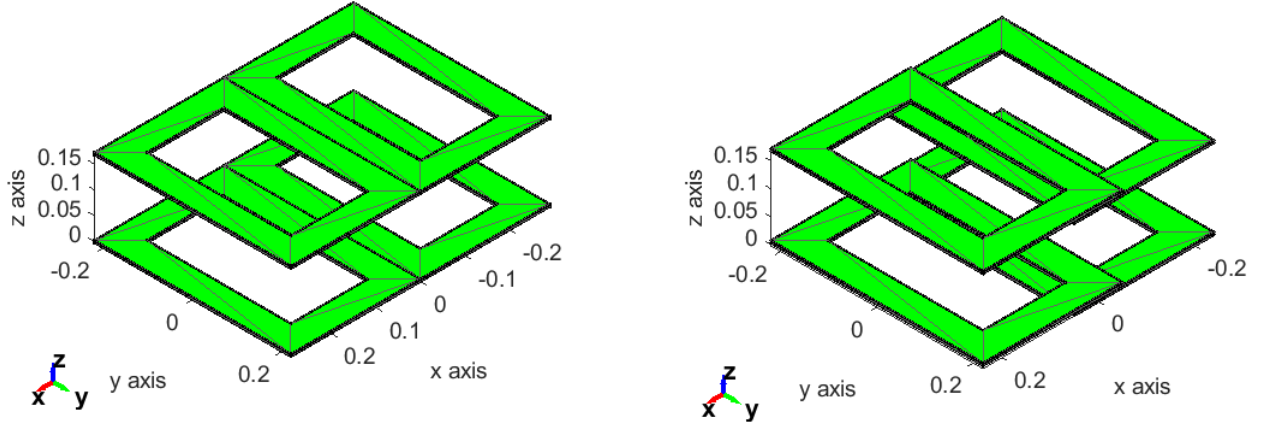


Figure 4.6: Double-D and and DD overlapped

The polarized coils are composed by two basic rectangular coils, this system is described by the follow equations:

$$\begin{cases} \hat{V}_1 = j\omega(L_{11}\hat{I}_1 + L_{12}\hat{I}_2 + L_{13}\hat{I}_3 + L_{14}\hat{I}_4) \\ \hat{V}_2 = j\omega(L_{21}\hat{I}_1 + L_{22}\hat{I}_2 + L_{23}\hat{I}_3 + L_{24}\hat{I}_4) \\ \hat{V}_3 = j\omega(L_{31}\hat{I}_1 + L_{32}\hat{I}_2 + L_{33}\hat{I}_3 + L_{34}\hat{I}_4) \\ \hat{V}_4 = j\omega(L_{41}\hat{I}_1 + L_{42}\hat{I}_2 + L_{43}\hat{I}_3 + L_{44}\hat{I}_4) \end{cases} \quad (4.4.3)$$

considering the two coils that form the polarized coil connected in series, it can be written:

$$\begin{cases} I_1 = I_2 = I_t \\ I_3 = I_4 = I_r \end{cases} \quad (4.4.4)$$

gathering the same current terms the equation can be re-written as:

$$\begin{cases} \hat{V}_1 = j\omega[(L_{11} + L_{12})\hat{I}_t + (L_{13} + L_{14})\hat{I}_r] \\ \hat{V}_2 = j\omega[(L_{21} + L_{22})\hat{I}_t + (L_{23} + L_{24})\hat{I}_r] \\ \hat{V}_3 = j\omega[(L_{31} + L_{32})\hat{I}_t + (L_{33} + L_{34})\hat{I}_r] \\ \hat{V}_4 = j\omega[(L_{41} + L_{42})\hat{I}_t + (L_{43} + L_{44})\hat{I}_r] \end{cases} \quad (4.4.5)$$

moreover, if the coils are in series, each coil voltage can be added up:

$$\begin{cases} V_1 + V_2 = V_t \\ V_3 + V_4 = V_r \end{cases} \quad (4.4.6)$$

obtaining:

$$\begin{cases} \hat{V}_t = j\omega[(L_{11} + L_{12} + L_{21} + L_{22})\hat{I}_t + (L_{13} + L_{14} + L_{23} + L_{24})\hat{I}_r] \\ \hat{V}_r = j\omega[(L_{31} + L_{32} + L_{41} + L_{43})\hat{I}_t + (L_{23} + L_{24} + L_{43} + L_{44})\hat{I}_r] \end{cases} \quad (4.4.7)$$

putting:

$$\begin{cases} L_{11} + L_{12} + L_{21} + L_{22} = L_t \\ L_{23} + L_{24} + L_{43} = L_r + L_{44} \\ L_{13} + L_{14} + L_{23} + L_{24} = L_{31} + L_{32} + L_{41} + L_{43} = M \end{cases} \quad (4.4.8)$$

the final equations result:

$$\begin{cases} \hat{V}_t = j\omega(L_t\hat{I}_1 + M\hat{I}_2) \\ \hat{V}_r = j\omega(M\hat{I}_1 + L_r\hat{I}_2) \end{cases} \quad (4.4.9)$$

For these two coils the same procedure explained in the bullet points is applied but, since they behave as two rectangular coils, it is necessary to compute all the self and mutual inductance between each rectangular coil. In order to formulate the final equivalent coil inductance.

Double-D overlap

For the double-D overlapped coil the suitable overlap distance have to be calculated.

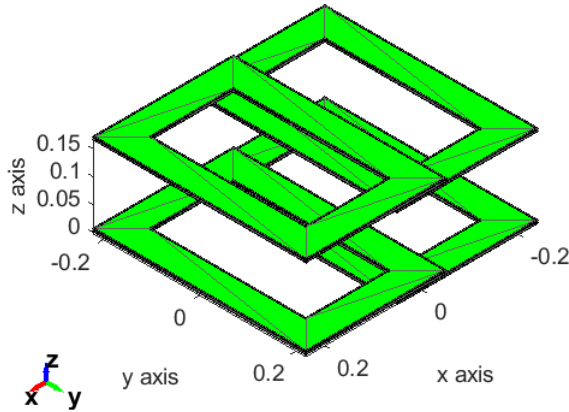


Figure 4.7: DD overlapped geometry

This configuration is substantially based on the DD topology. Nevertheless, the overlap of the coils offers some additional interesting benefit. In fact, overlapping them, it is possible to reduce, ideally to zero, the mutual inductance between the two rectangular coils. Reducing the mutual inductance mainly gave the advantages to drive the coil in different ways without worry about their interaction.

The overlap distance clearly cannot be the same for all coils, but it depends of the coil dimensions. So, the right overlap distance has to be calculated for the chosen coils.

The condition of zero mutual inductance has been found using a for loop. It gradually overlaps the two coils and calculate the mutual inductance at each iteration. The result in 4.8 confirm the existence of an overlap distance that guarantees the absence of mutual coupling between the two D of the coil.

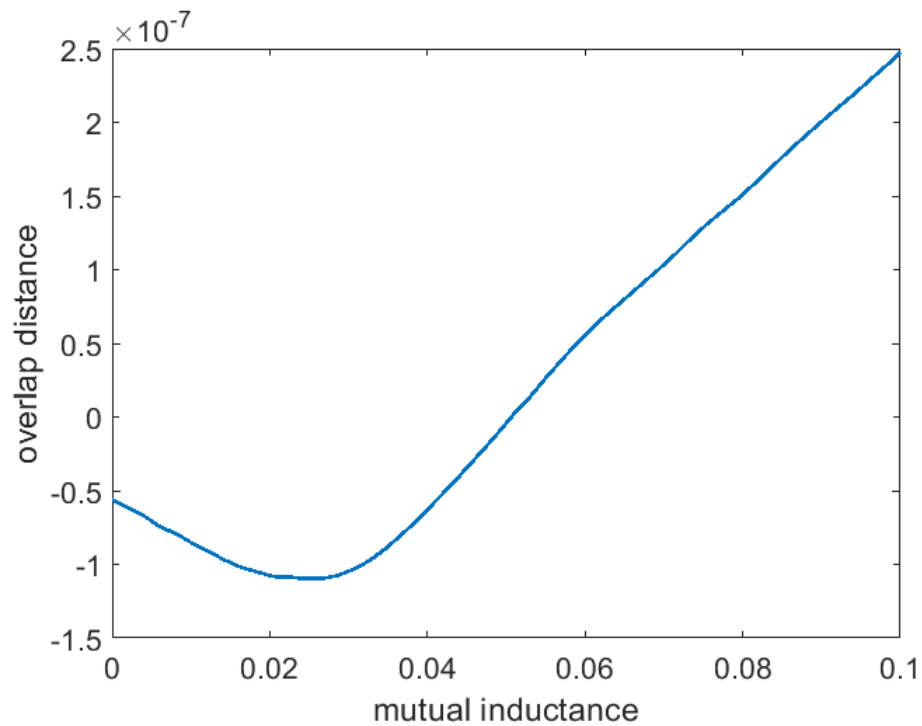


Figure 4.8: Zero mutual inductance distance

Once the value of zero mutual is found, exploiting a linear interpolation, the corresponding overlap distance has been found. It is equal to: $OV-d=0.0502$ m. The receiver and the transmitter have the same dimensions, so the overlap distance is the same.

4.4.3 Double-D quadrature coil

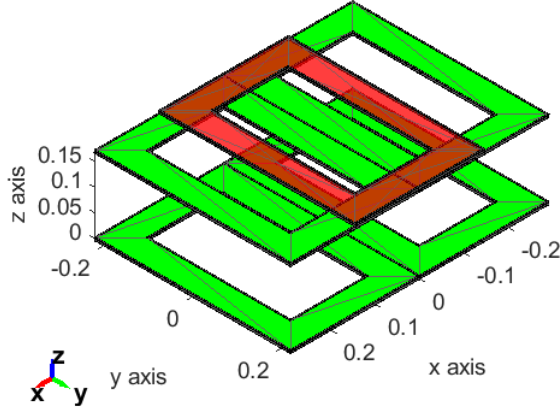


Figure 4.9: DDQ coil geometry

In the previous system of equations it was possible to exploit the series circuit characteristics to gather the same current terms. This allows to add up the voltage terms and define the self and mutual inductance terms. In the double-D quadrature coil equations appear the terms linked with the quadrature coil. These terms do not allow to use the series connection properties to carry out the same procedure. For this reason this coil needs further steps to define the receiver and transmitter self and mutual inductance.

The system equations are:

$$\begin{cases} \hat{V}_1 = j\omega(L_{11}I_1 + L_{12}I_2 + L_{13}I_3 + L_{14}I_4 + L_{1q}I_5) \\ \hat{V}_2 = j\omega(L_{21}I_1 + L_{22}I_2 + L_{23}I_3 + L_{24}I_4 + L_{2q}I_5) \\ \hat{V}_3 = j\omega(L_{31}I_1 + L_{32}I_2 + L_{33}I_3 + L_{34}I_4 + L_{3q}I_5) \\ \hat{V}_4 = j\omega(L_{41}I_1 + L_{42}I_2 + L_{43}I_3 + L_{44}I_4 + L_{4q}I_5) \\ \hat{V}_5 = j\omega(L_{51}I_1 + L_{52}I_2 + L_{53}I_3 + L_{54}I_4 + L_{55}I_5) \end{cases} \quad (4.4.10)$$

knowing the series circuit relations:

$$\begin{cases} I_1 = I_2 = I_t \\ I_3 = I_4 = I_t \end{cases} \quad (4.4.11)$$

$$\begin{cases} \hat{V}_1 = j\omega[(L_{11} + L_{12})I_t + (L_{13} + L_{14})I_r + L_{1q}I_5] \\ \hat{V}_2 = j\omega[(L_{21} + L_{22})I_t + (L_{23} + L_{24})I_r + L_{2q}I_5] \\ \hat{V}_3 = j\omega[(L_{31} + L_{32})I_t + (L_{33} + L_{34})I_r + L_{3q}I_5] \\ \hat{V}_4 = j\omega[(L_{41} + L_{42})I_t + (L_{43} + L_{44})I_r + L_{4q}I_5] \\ \hat{V}_5 = j\omega[(L_{51} + L_{52})I_t + (L_{53} + L_{54})I_r + L_{55}I_5] \end{cases} \quad (4.4.12)$$

using:

$$\begin{cases} V_1 + V_2 = V_t \\ V_3 + V_4 = V_r \end{cases} \quad (4.4.13)$$

$$\begin{cases} \hat{V}_t = j\omega[(L_{11} + L_{12} + L_{21} + L_{22})I_t + (L_{13} + L_{14} + L_{23} + L_{24})I_r + (L_{15} + L_{25})I_5] \\ \hat{V}_r = j\omega[(L_{31} + L_{32} + L_{41} + L_{42})I_t + (L_{33} + L_{34} + L_{43} + L_{44})I_r + (L_{35} + L_{45})I_5] \\ \hat{V}_5 = j\omega[(L_{51} + L_{52})I_t + (L_{53} + L_{54})I_r + L_{55}I_5] \end{cases} \quad (4.4.14)$$

and imposing:

$$\begin{cases} L_t = L_{11} + L_{12} + L_{21} + L_{22} \\ M_{tr} = L_{13} + L_{14} + L_{23} + L_{24} \\ M_{rt} = L_{31} + L_{32} + L_{41} + L_{42} \\ L_r = L_{33} + L_{34} + L_{43} + L_{44} \\ M_{tq} = L_{15} + L_{25} \\ M_{rq} = L_{35} + L_{45} \\ M_{qt} = L_{51} + L_{52} \\ M_{qr} = L_{53} + L_{54} \\ L_q = L_{55} \end{cases} \quad (4.4.15)$$

the matrix system can be written as:

$$\begin{bmatrix} \hat{V}_t \\ \hat{V}_r \\ \hat{V}_q \end{bmatrix} = j\omega \begin{bmatrix} L_t & M_{tr} & M_{tq} \\ M_{rt} & L_r & M_{rq} \\ M_{qt} & M_{qr} & L_q \end{bmatrix} \begin{bmatrix} I_t \\ I_r \\ I_q \end{bmatrix} \quad (4.4.16)$$

At this point an admittance matrix is defined, such that $P = M^{-1}$:

$$\begin{bmatrix} \hat{I}_t \\ \hat{I}_r \\ \hat{I}_q \end{bmatrix} = \frac{1}{j\omega} \begin{bmatrix} P_t & P_{tr} & P_{tq} \\ P_{rt} & P_r & P_{rq} \\ P_{qt} & P_{qr} & P_q \end{bmatrix} \begin{bmatrix} V_t \\ V_r \\ V_q \end{bmatrix} \quad (4.4.17)$$

considering the double-D receiver and the quadrature coil connected in parallel, the follow relation can be used:

$$I_s = I_r + I_q$$

where:

- I_s is the equivalent DDQ receiver coil current
- I_r is the double-D receiver coil current
- I_q is the quadrature coil current

adding up the last two equation it can be obtained:

$$\begin{bmatrix} \hat{I}_t \\ \hat{I}_s \end{bmatrix} = \frac{1}{j\omega} \begin{bmatrix} P_t & (P_{tr} + P_{tq}) \\ (P_{rt} + P_{qt}) & (P_r + P_{qr} + P_{rq} + P_q) \end{bmatrix} \begin{bmatrix} V_t \\ V_s \end{bmatrix} \quad (4.4.18)$$

putting:

$$\begin{cases} P_{ts} = P_{tr} + P_{tq} \\ P_{st} = P_{rt} + P_{qt} \\ P_s = P_r + P_{qr} + P_{rq} + P_q \end{cases} \quad (4.4.19)$$

and re-writing the equations:

$$\begin{bmatrix} \hat{I}_t \\ \hat{I}_s \end{bmatrix} = \frac{1}{j\omega} \begin{bmatrix} P_t & P_{ts} \\ P_{st} & P_s \end{bmatrix} \begin{bmatrix} V_t \\ V_s \end{bmatrix} \quad (4.4.20)$$

re-inverting the P matrix the inductances matrix can be written:

$$\begin{bmatrix} \hat{V}_t \\ \hat{V}_s \end{bmatrix} = j\omega \begin{bmatrix} L_t & M \\ M & L_s \end{bmatrix} \begin{bmatrix} I_t \\ I_s \end{bmatrix} \quad (4.4.21)$$

where:

- L_t is the transmitter's self-inductance
- L_s is the DDQ receiver's equivalent inductance
- M is the mutual inductance between the previous coil

4.4.4 Additional geometries

The previously presented geometries have been found in literature and are certainly the most used, but exploiting the overlapping technique new forms of coils, based on the previous geometries, can be proposed.

Double-D coil types

Others two coil topologies can be derived by the double-D coil.

The first one, is obtained overlapping the receiver coil, as depicted in 4.10

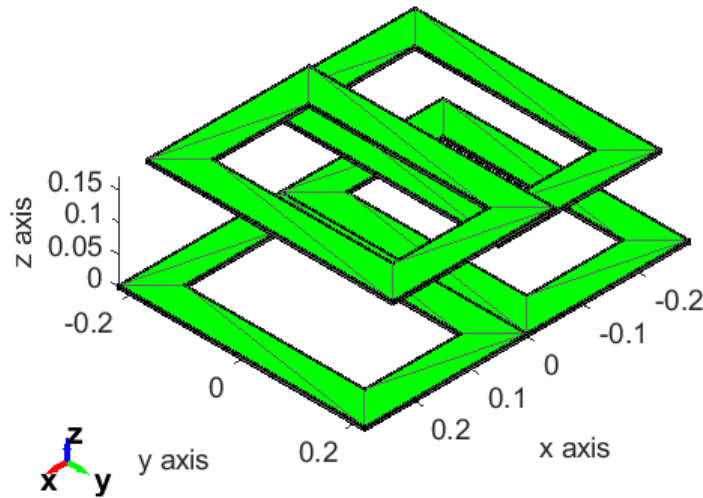


Figure 4.10: Double-D receiver overlapped coil

The same can be made for the transmitter coil, as depicted in 4.11

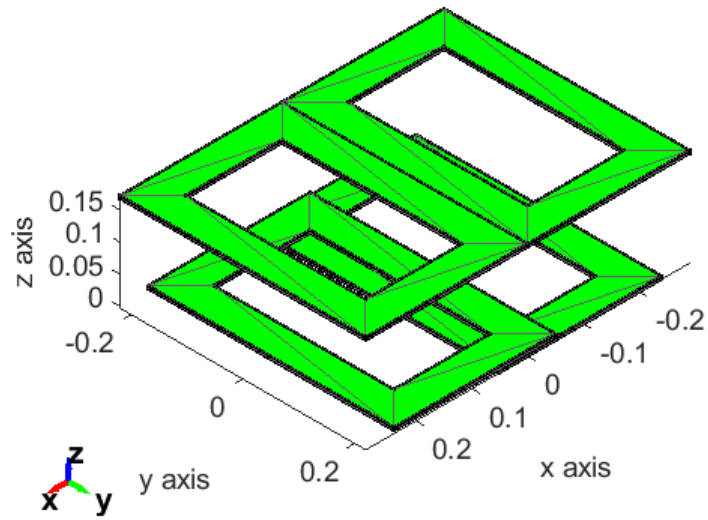


Figure 4.11: Double-D transmitter overlapped coil

The overlap distance applied to these coils is the same one found in the paragraph 1.3.3.

Coil derived from the DDQ coil

The same procedure can be made for DDQ coil. Overlapping the transmitter the geometry in fig. 4.12 can be obtained.

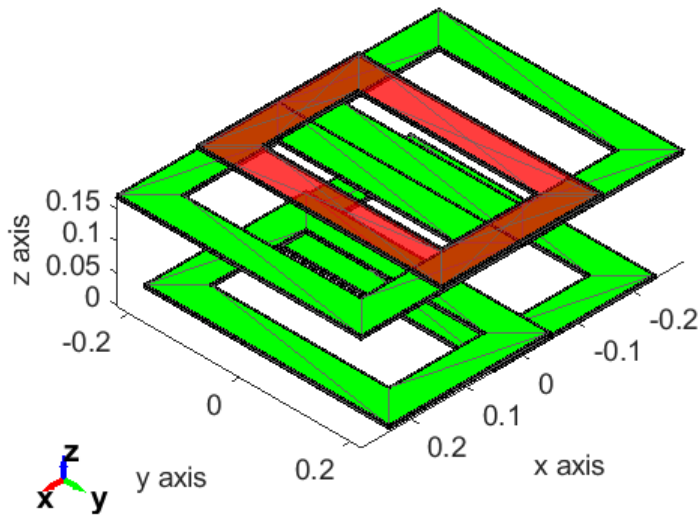


Figure 4.12: DDQ transmitter overlapped coil

instead, overlapping the receiver the geometry in fig. 4.13

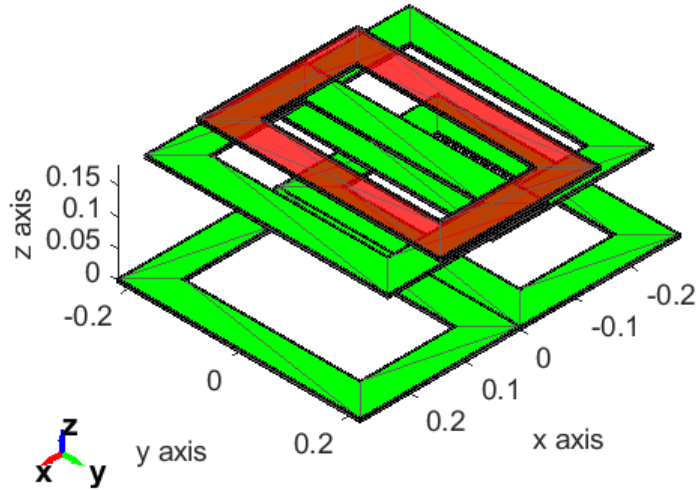


Figure 4.13: DDQ receiver overlapped coil

While, overlapping both receiver and transmitter the geometry in fig. 4.14

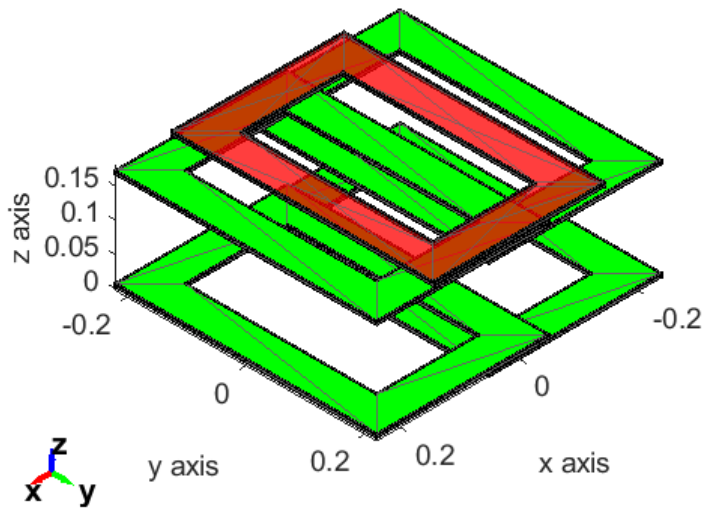


Figure 4.14: DDQ receiver and transmitter coils overlapped

These coils combination are analyzed to investigate if without changing the coil geometries, but simply overlapping them, it is possible to obtain some advantages, in terms of: coupling factor k , better behavior to misalignment and a better magnetic field shape.

4.4.5 Coupling factor k representation

In this section the criteria at the basic of the coupling factor k evaluation will be discussed. Basically, this section aims to understand how the coupling factor change under different working conditions. Four working condition will be analyzed: no misalignment, air-gap variation, x and y displacement.

The SAE J2954 is taken as reference to set the air-gap for the no-misalignment condition and the range of variation for the simulation at different air-gaps.

The SAE J2954 defines different distances between each element of the system of coils. The main one is the vehicle assembly (VA) coil ground clearance, as in 4.15. The reference uses this distance to define the Z-classes reported in table 4.2. The reference aim is that a ground assembly (GA) have to operate for all the z values of the Z-classes.

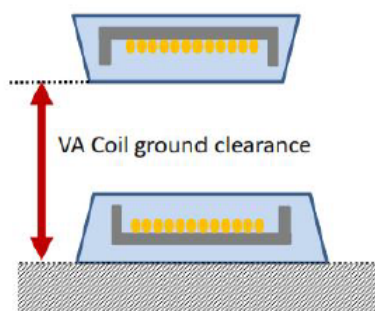


Figure 4.15: Coil ground clearance [12]

Z-Class	VA Coil ground clearance range (mm)
Z1	100-150
Z2	140-210
Z3	170-250

Table 4.2: Z-Classes defined in the SAE J2954 [12]

No misalignment

The first comparison calculate the coupling factor of each geometry with transmitter and receiver in a centered position. The two coils are at a respectively distance of 170 mm. This distance has been chosen because it is an average distance between the previously defined Z-classes. The results of the simulations are reported in a bar chart.

Air-gap variation

In a real IPT application the air-gap between the transmitter and the receiver can vary for different reasons, for example:

- the road is not perfectly flat
- the transmitter can be an above or under the ground surface
- the receiver can be mounted on different vehicles: BUS, SUV, sedan or a VAN.

For these reasons the coil coupling variation is investigated setting an air-gap variation from 100 mm to 300 mm. These values are referred to the table 4.2. The upper limit is beyond 250 mm because in literature higher distances than this limit have been analyzed. Anyway, 300 mm is a good compromise, because beyond 300 mm the values of k are too low.

The air-gap range (100-300 mm) is divided in 20 values to build up the outputs. To extrapolate as much information as possible the results are represented in two way:

First, the results are reported in a table that contains all the obtained values of k normalized with respect to the maximum value of k among all the values. In this way, each table value, represent a kind of percentage with respect to the maximum value of k that can be obtained.

Secondly, the same normalized values are plotted superimposing all the graphs of each geometry in one figure. In this way, it is possible to visualize and compare every coil reaction to the progressively higher distance directly, in a visual way.

X and Y misalignment

It is common experience that a vehicle cannot travel along the road maintaining a perfect alignment within the lane for all the travel. Likewise, for the static charge, when the vehicle is parked it is not perfectly aligned within the parking space. For these reasons a real IPT application must take into account a possible misalignment between the receiver and the transmitter. A simulation of this phenomenon is carried out gradually shifting the receiver coil with respect to the transmitter. The two coils are shifted until a distance $2R_{eq}$ is reached. Where R_{eq} is the radius of the circle inscribing the rectangular coil, as shown in 4.16

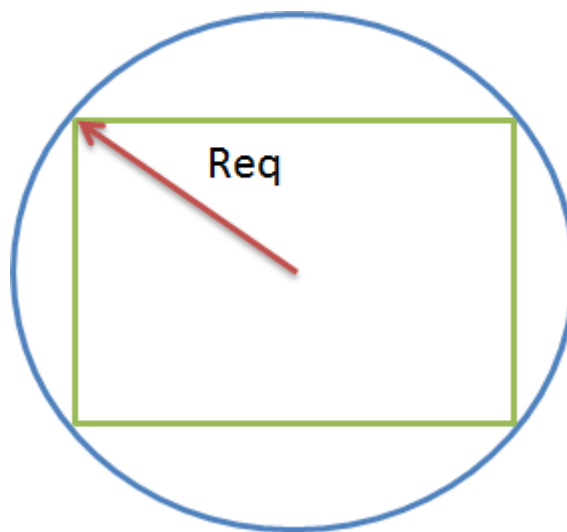


Figure 4.16: Equivalent radius

These same misalignment procedure is carried out in both x and y direction, as depicted in 4.17

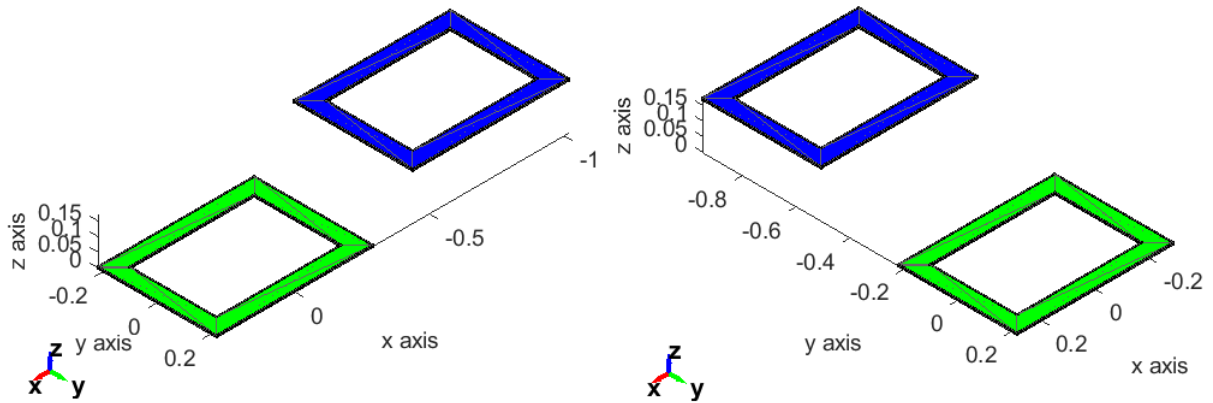


Figure 4.17: Maximum x and y coils misalignment

The k values obtained are normalized with respect to the maximum value of k of all coils respectively for the x and y displacement.

The results are represented in two ways:

- Superimposing each coil plot on the same figure
- Reporting in a bar chart the distance at which each coil value of k goes negative

4.5 Magnetic flux density B

The magnetic flux density B is another important parameter that allows to understand different coil behaviors. It is an important factor for the IPT system because it is linked with the magnetic coupling and therefore with the power transferred. Anyway, it is very important for the stray field issue and the limitation of humans exposure to it. In fact, the International Commission on Non-Ionizing Radiation Protection (ICNIRP)[3] released particular specification to limit and prevent the human exposure to a time-varying EMF. The exposure to an EMF at frequency lower than 100 kHz can cause: annoyance, surface electric-charge, stimulation of central and peripheral nervous tissue, and the induction of phosphenes. For this reasons, the reference, in 2010, indicates to do not expose the body to an avarage RMS flux density of 27 μT

In order to generate a magnetic field, a current have to flow in each coil. The two currents that flow in both transmitter and receiver can be defined referring to the equivalent circuit in 4.18. In particular in order to define them an equivalent load R_L and a compensation topology should be decided. Anyway, the thesis aim is to carry out an as generic as possible comparison. For this reason the system is not compensated and a unit current is imposed in each coil.

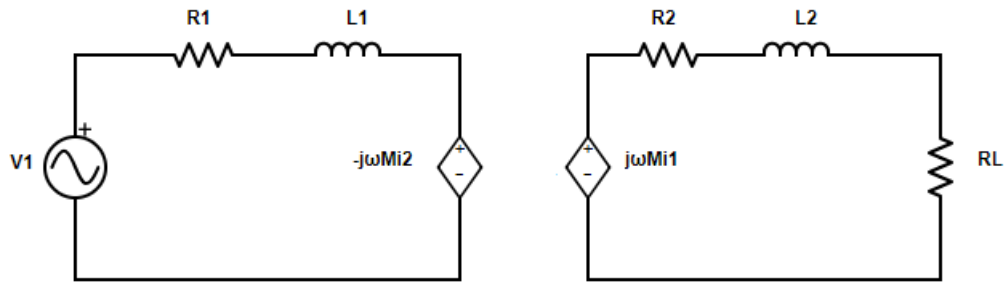


Figure 4.18: IPT equivalent circuit

Moreover, referring to the series compensation topology in fig. 4.19

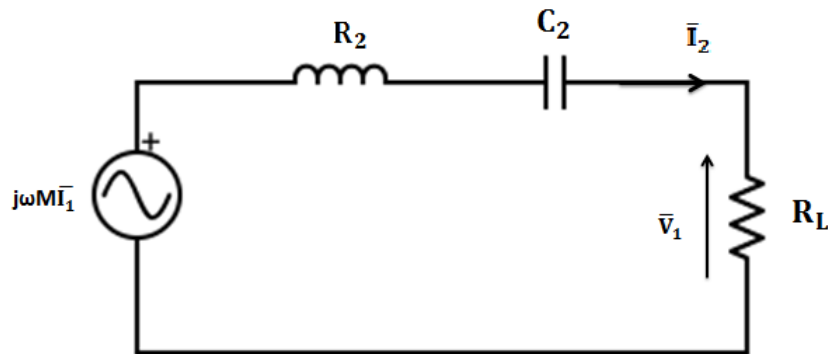


Figure 4.19: Series compensation

for the resonance condition $\omega = \omega_0$, it can be written:

$$\hat{V}_2 = R_2 \hat{I}_2 = j\omega M \hat{I}_1 \quad (4.5.1)$$

the phase of between the transmitter and receiver current are linked by the relation 4.5.2

$$\angle \hat{I}_2 = \angle \hat{I}_1 + \frac{\pi}{2} \quad (4.5.2)$$

Considering a parallel compensation 4.20

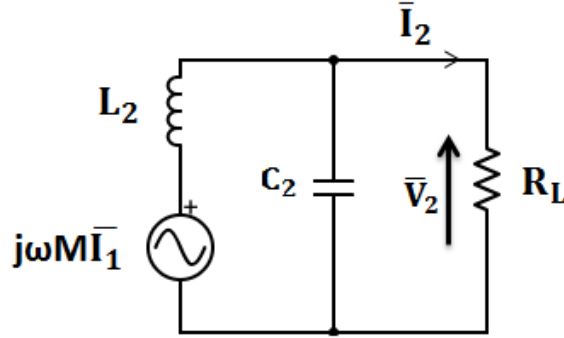


Figure 4.20: Parallel compensation

a Norton equivalent circuit can be drawn:

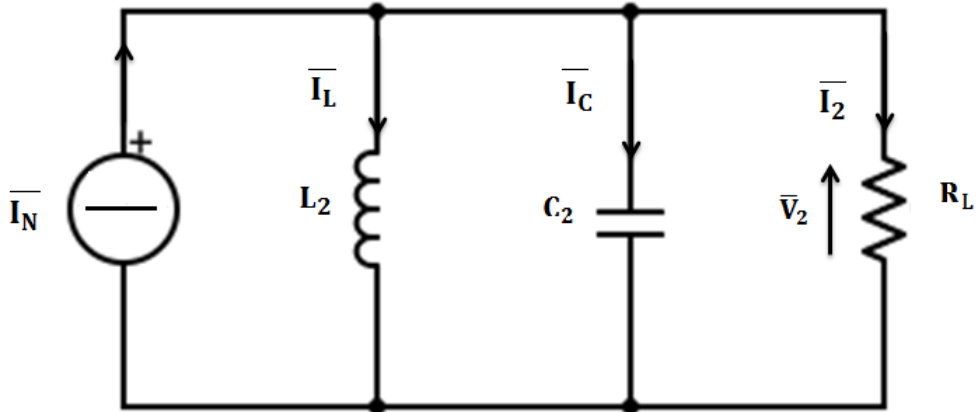


Figure 4.21: Norton equivalent circuit

where:

$$\hat{I}_N = \frac{j\omega M \hat{I}_1}{j\omega L_2} = \frac{M}{L_2} \hat{I}_1 \quad (4.5.3)$$

for the resonant condition $\omega = \omega_0$:

$$\hat{I}_2 = \hat{I}_N \quad (4.5.4)$$

and

$$\hat{V}_2 = R_L \hat{I}_2 \quad (4.5.5)$$

the inductor current can be written as:

$$\hat{I}_L = \frac{\hat{V}_2}{j\omega L_2} \quad (4.5.6)$$

so, I_L is:

$$\hat{I}_L = \frac{\hat{V}_2}{j\omega L_2} = R_L \frac{M}{L_2} \frac{1}{j\omega L_2} \hat{I}_1 \quad (4.5.7)$$

the phase relation between the two currents is:

$$\angle \hat{I}_L = \angle \hat{I}_1 - \frac{\pi}{2} \quad (4.5.8)$$

Therefore, for the magnetic flux density calculation a unit real current is imposed to the transmitter and a unit imaginary current to the receiver.

The magnetic flux density B is calculated on three different planes, as depicted in 4.22. Ones positioned in the receiver plane, ones in the middle of the air-gap and the third in the receiver plane. Evaluating these three different planes it is possible to better evaluate the field shape and its variation between the two coils. The three planes has dimension of $4R_{circ}$ for each side. Where R_{circ} is the circular coil radius.

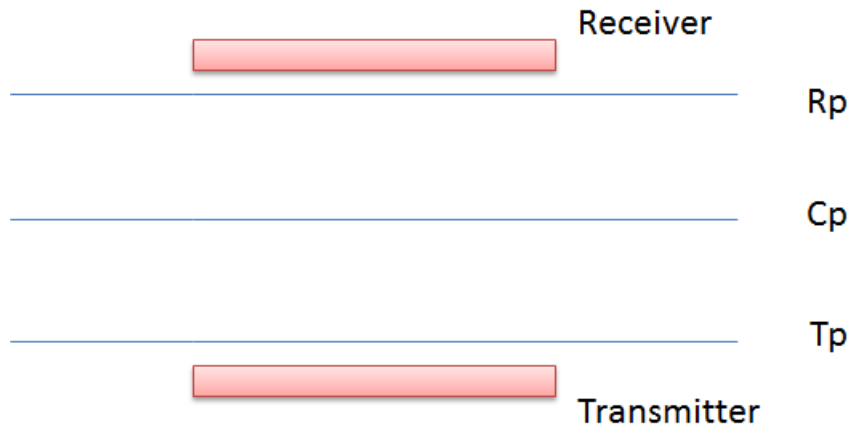


Figure 4.22: Magnetic flux density B plane planes. Rp: receiver plane; Cp: central plane; Tp: transmitter plane

Plot-line Field

The magnetic flux density is computed also on x and y direction starting from the coil center, as in 4.23. This further field representation is used to find how far from the coil center each geometry goes under a B value of $27 \mu\text{T}$. In this way it is possible to obtain informations in reference to the human exposure issue.

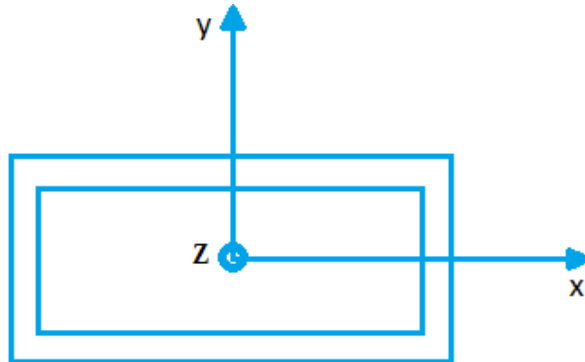


Figure 4.23: Axis reference system

the field trend is represented from the coil center within a distance of two times the equivalent radius corresponding to the coil area.

In this case a current of 10 A is imposed to the transmitter and j10 A to the receiver. This current has been used because is representative for WPT1 types of system. This magnetic flux density calculation is carried out for x and y directions and for the three planes previously defined.

Chapter 5

Comparison results

5.1 Comparison results

In this chapter the founded results will be showed , exploiting different types of representation, such as: bar charts, plot-line graph types and contour graph types. First have been reported the coupling factor results and secondly the the magnetic flux results.

5.2 Coupling factor k

In this paragraph, the coupling factor k results will be represented splitting them into four different sections, in order to visualize the coil behaviors for the optimal coil positions (centered position) and how they reacts to vertical and horizontal misalignment.

5.2.1 No misalignment

In figure 5.1 each coil value of k is represented. It is computed for the optimal air-gap of 170 mm. The bar-chart allows to immediately see the main differences between the coils.

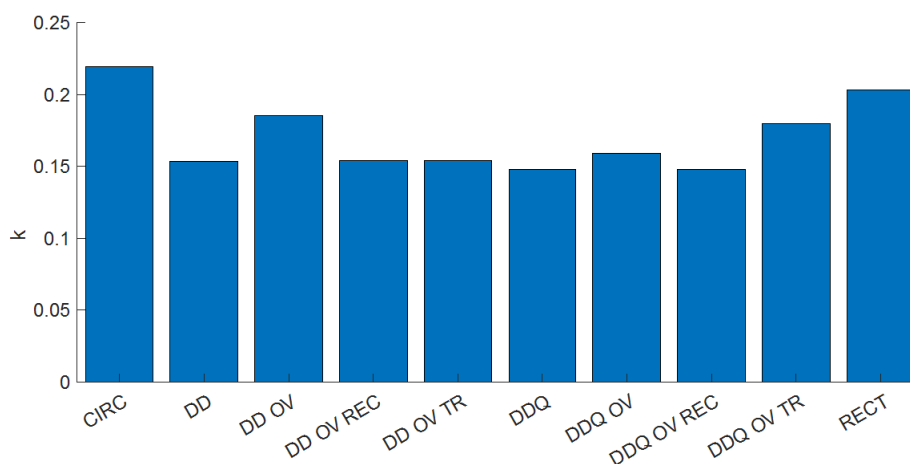


Figure 5.1: Values of k for no-misalignment condition

Looking at the chart, the circular coil reach the highest values with a coupling of $k_{circ} = 0.2195$, it is followed by the rectangular one with a slightly lower value of $k_{rect} =$

0.2029. These two results basically confirm all the studies previously analyzed in the state of the art and the others comparison studies already presented in literature. A surprising data instead, comes from the double-D overlapped coil. This one has a value of k of $k_{DD_{ov}} = 0.1855$, this result can be explained thinking of the k expression: at the denominator it has the product, under square root, of the two coil self-inductance. For the double-D coil, it is the sum of each "rectangular" coil plus the two mutual inductance between them. Overlapping them to two mutual inductance goes to zero obtaining a low value of self-inductance and consequently a low value of the denominator. For this reason the value of k is higher than the normal double-D. The same result has been obtained for the DDQ coil with the transmitter coil overlapped. All the others coil have similar values of k between 0.14 and 0.16. An information that comes out from this chart is that doing an overlap on both receiver and transmitter gives higher coupling factor than doing that only on one coil.

5.2.2 Values of k varying the air-gap

In this paragraph, it will be seen how the coupling factor changes varying the air-gap between the receiver and the transmitter. The first figure shows a table reporting the values of k normalized with respect the highest value of k obtained for 20 different air-gap:

(m)	circ	rect	DD	DD _{ov}	DDQ	DDQ _{ov_tr}	DDQ _{ov}	DD _{ov_tr}	DD _{ov_rec}	DDQ _{ov_rec}
0.1000	1	0.9384	0.7446	0.8519	0.6598	0.8377	0.7599	0.6893	0.6894	0.4971
0.1105	0.9230	0.8635	0.6781	0.7807	0.6110	0.7725	0.6968	0.6390	0.6391	0.4667
0.1211	0.8541	0.7969	0.6201	0.7176	0.5674	0.7132	0.6402	0.5933	0.5934	0.4385
0.1316	0.7921	0.7373	0.5692	0.6612	0.5281	0.6594	0.5894	0.5517	0.5518	0.4122
0.1421	0.7360	0.6837	0.5241	0.6106	0.4925	0.6105	0.5436	0.5137	0.5138	0.3876
0.1526	0.6852	0.6353	0.4840	0.5649	0.4601	0.5660	0.5021	0.4790	0.4791	0.3647
0.1632	0.6389	0.5913	0.4481	0.5236	0.4303	0.5253	0.4645	0.4472	0.4473	0.3432
0.1737	0.5966	0.5513	0.4159	0.4860	0.4030	0.4882	0.4303	0.4181	0.4181	0.3232
0.1842	0.5578	0.5148	0.3868	0.4518	0.3778	0.4542	0.3992	0.3912	0.3912	0.3044
0.1947	0.5223	0.4813	0.3604	0.4206	0.3546	0.4231	0.3707	0.3665	0.3665	0.2868
0.2053	0.4895	0.4506	0.3365	0.3921	0.3330	0.3945	0.3448	0.3437	0.3437	0.2703
0.2158	0.4593	0.4224	0.3146	0.3659	0.3131	0.3683	0.3210	0.3226	0.3226	0.2548
0.2263	0.4314	0.3964	0.2947	0.3418	0.2946	0.3442	0.2992	0.3031	0.3031	0.2404
0.2368	0.4057	0.3724	0.2764	0.3197	0.2774	0.3220	0.2792	0.2850	0.2850	0.2268
0.2474	0.3818	0.3502	0.2595	0.2993	0.2614	0.3015	0.2609	0.2683	0.2683	0.2141
0.2579	0.3596	0.3296	0.2440	0.2805	0.2465	0.2826	0.2439	0.2527	0.2527	0.2022
0.2684	0.3390	0.3106	0.2297	0.2631	0.2326	0.2651	0.2284	0.2382	0.2382	0.1911
0.2789	0.3198	0.2929	0.2165	0.2471	0.2196	0.2490	0.2140	0.2247	0.2247	0.1806
0.2895	0.3020	0.2764	0.2043	0.2322	0.2075	0.2340	0.2007	0.2122	0.2122	0.1709
0.3000	0.2854	0.2611	0.1929	0.2184	0.1962	0.2201	0.1884	0.2005	0.2005	0.1617

Figure 5.2: Normalized values of k varying the air-gap

As expected, the highest coupling value is reached by the circular coil at the minimum distance of 100 mm. In fact, its normalized value is 1 and it is the reference value with respect to all the other values have been normalized. The rectangular coil confirms its good performance loosing only, at the minimum air-gap, a little bit more than 6% with respect to the circular coil. Even when the two coils are at the maximum air-gap their coupling factors are higher than the others respectively about the 28% and 26%.

Another two interesting coils are the double-D overlapped (DD_{ov}) and the DDQ with the overlapped transmitter (DDQ_{ov_tr}) these two coils have a coupling value about a 10% lower than the highest coupling value, however both have an overall better behavior respect to the other coils. Looking at the first and the last two coupling values, it can be seen that the DDQ_{ov_tr} start with lower value than DD_{ov} , but the last value is slightly

better. So, it has a better reaction to the air-gap increasing. In red has been highlighted the lowest values giving by the DDQ with the receiver overlapped ($DDQ_{ov.rec}$), it starts with about 50% of the maximum k and goes down to about 16% at the maximum air-gap.

The same results have been superimposed on the same figure producing the following graph. The red dashed line was drawn to remember the distance used for the nominal misalignment case (170 mm):

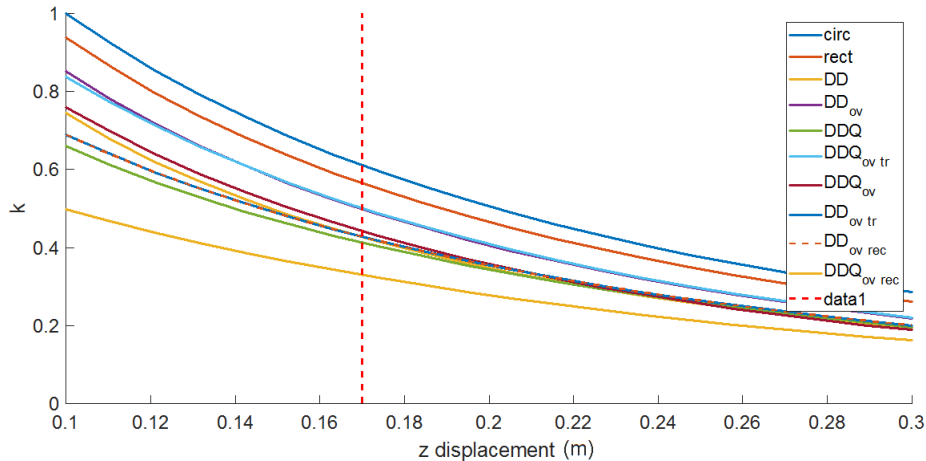


Figure 5.3: Normalized values of k changing the air-gap

Analyzing the graph, it is clear that the rectangular and circular coils have better performance, with the circular coil, in particular, that is well seconded from the rectangular one. As has been showed before, the $DDQ_{ov.tr}$ coil has a slightly better behavior at higher air-gap, in fact the light blue curve keeps higher coupling values above 140 mm of air-gap. Another good performance is given by both $DD_{ov.rec}$ and $DD_{ov.tr}$, their curves are completely superimposed forming the dashed orange and blue curve. They have a lower coupling value for the minimum air-gap with respect to the $DDQ_{ov.rec}$ (beige color) and the DDQ_{ov} (amaranth color) but, increasing the air-gap, they has kept a high coupling values overcoming the last two mentioned coils. The same performance, with slightly low values of k is given by the DDQ coil. From the results highlighted above, seems that, for DD coil, overlap both transmitter and receiver allows to reach higher coupling values, as explained before. In general, to overlap at least the transmitter or the receiver help to keep high coupling value for a good range of air-gap. For the DDQ type of coil, seems that to overlap the transmitter allows bigger couplings than overlapping the receiver. This has had a bad impact on the coupling factor. Overlapping both the transmitter and the receiver brings to a medium behavior between the previous situation. Finally, the DDQ has medium values of coupling with a good response to air-gap increase.

5.2.3 Coils behavior to x misalignment

In this section the coil reaction to horizontal misalignment, in x direction, will be analyzed. The x direction is perpendicular to the travel vehicle direction. The results are showed in 5.4

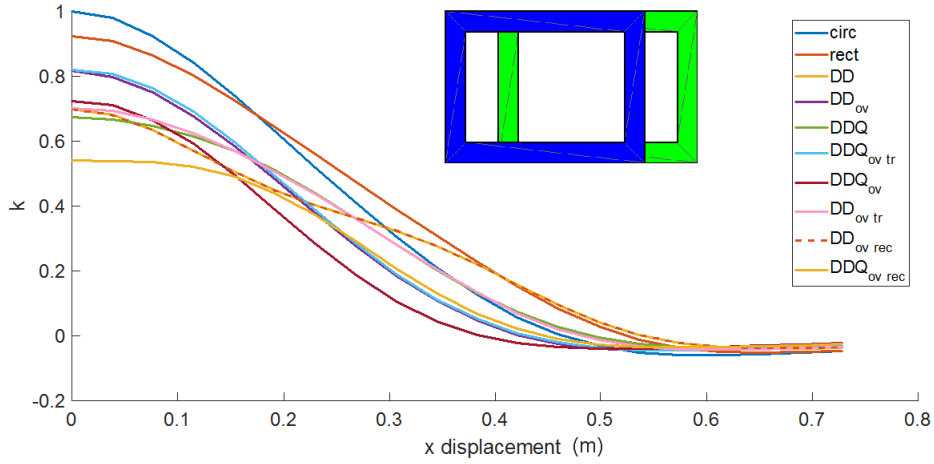


Figure 5.4: Normalized values of k changing x -displacement

Starting with circular and rectangular geometries: the circular one starts with the maximum value of k when it is aligned, but when the displacement progressively increase the circular coil loose its magnetic coupling quite soon, it is not tolerant to x misalignment. The rectangular coil starts as expected with a lower k value than circular coil, but it has greater tolerance to misalignment than the circular one. In fact, around a distance of 180 mm it keeps a good value of k , overcoming the circular coil. Another interesting result is given by the following geometries: DD_{ov} , DD_{ovtr} , DDQ , DDQ_{ovtr} . The DDQ_{ovtr} , in light blue, and the DD_{ov} , in violet, both start with the two highest values after the circular and rectangular geometry, but do not have a good reaction to misalignment, they loose their magnetic coupling with the same trend of the circular coil. Instead, the DD_{ovtr} coil, in pink, and the DDQ coil, in green, have a lower value of k with respect to the previous coils when they are aligned. While increasing the misalignment they are both able to keep a good magnetic coupling. In fact, around 180 mm, they overcome the first two coils curves. A surprising result has been found for the DD and DD_{ovrec} coils they have the good slope along the misalignment, keeping good values of k even for high values of misalignment. The DDQ_{ov} loose its magnetic coupling quite soon it does not have a good reaction to displacement.

From this comparison the two geometries that result the most suitable to work in misalignment conditions are: the rectangular and the DD (even with the overlapped receiver). The first one, keeps bigger k values for good part of the distance. While, DD and DD_{ovrec} , has a better slope averagely constant along the displacement.

The bar chart 5.5 is used to point-out which coil and at what distance falls to the value of zero coupling.

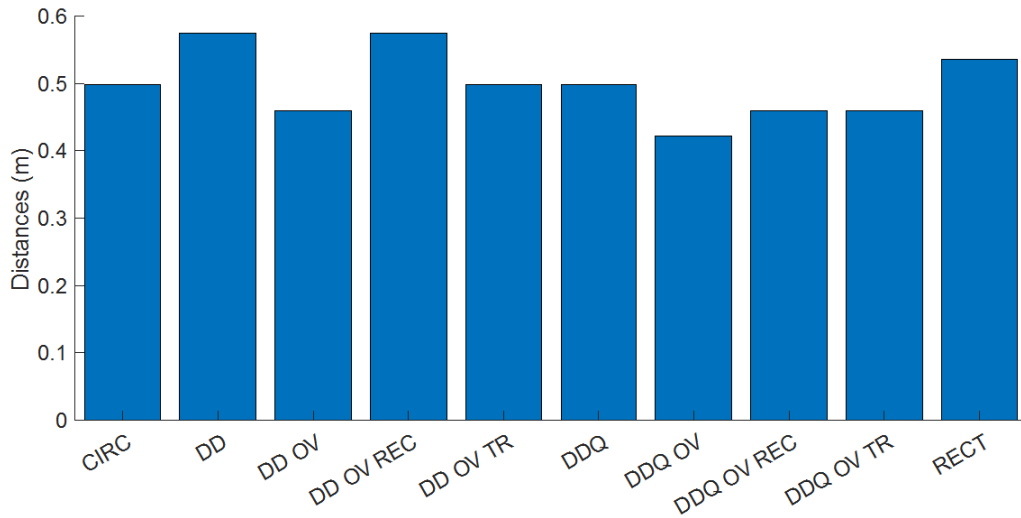


Figure 5.5: Distance at which there is zero coupling x-displacement

As can be immediately seen the two geometries that reach the higher distance from the coil center are: DD and DD_{ovrec} . They reach the zero coupling at around 0.58 m from the coil center. Immediately after them the rectangular coil (slight blue) has a good performance to x displacement, it goes to zero coupling at around 0.55 m. The DDQ_{OV} coil has the worst performance it goes to zero coupling at about 0.42 m.

5.2.4 Coils reaction to y misalignment

In this section the same results will be showed, but for the y-directions. The y-direction is the same as the vehicle travel direction.

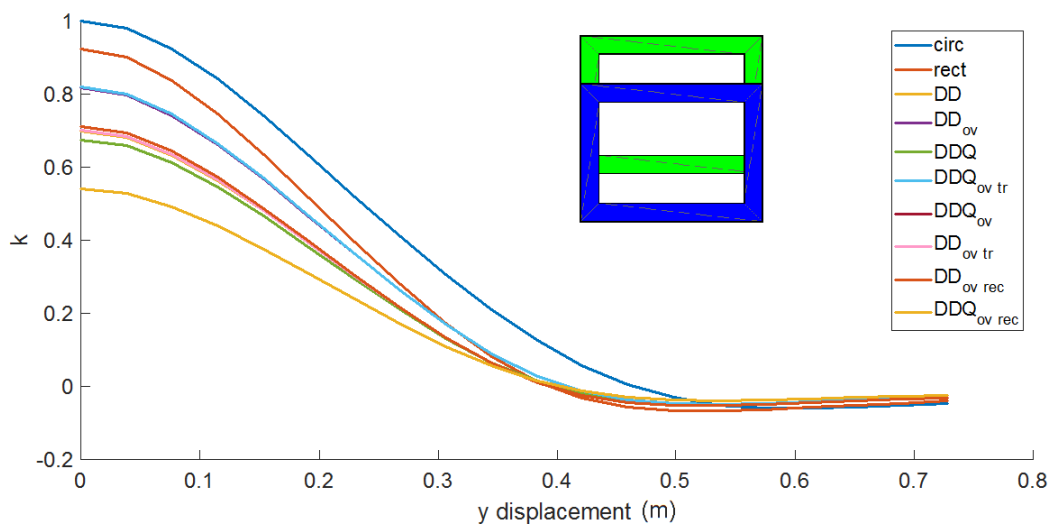


Figure 5.6: Normalized values of k changing y displacement

In this figure it can be noticed that the circular coil seems to have a better behavior to misalignment, but this conclusion it is not immediate. It should be considered that on y direction the rectangular coil has its short side, instead the distance from the coil center for the circular coil, is its radius for all directions. For this reason the circular coil seems to have a better coupling than others coils. This behavior worth for all rectangular coil type. All the polarized coil types has the same behavior because they all have the same coil side, therefore there are no particular points to highlight.

The bar chart is used to highlight when each coil reach the value of zero coupling.

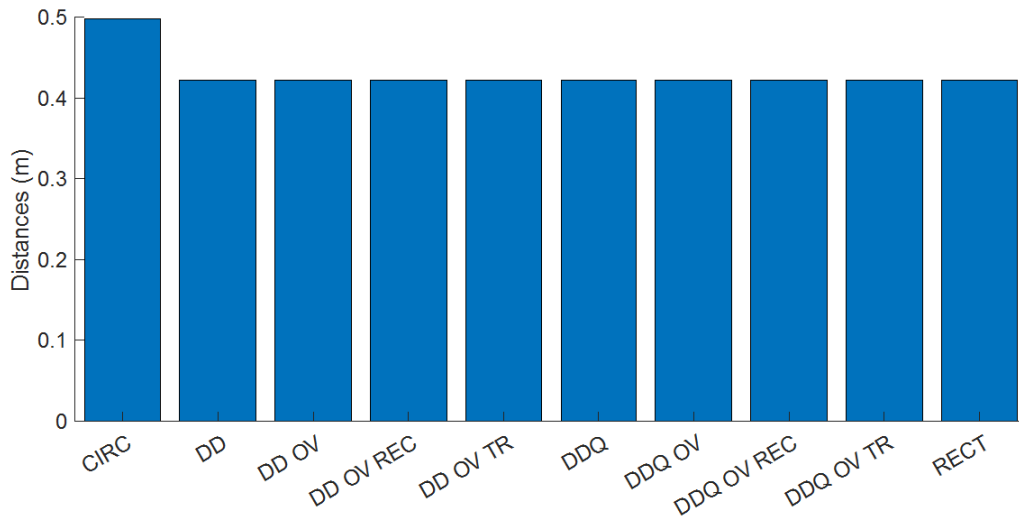


Figure 5.7: Distance at which each coil reaches the zero coupling

Looking at the graph the circular coil reaches the zero coupling condition at about 0.5 m. All the other coil reach the same condition at a distance of about 0.42 m from the coil center.

5.3 Magnetic flux density B

In this section the simulation results of magnetic flux density will be showed. In particular a series of contour figure will be showed to analyze the field shape on the central plane. Moreover, some plot-line and bar-chart type graphs will be reported to visualize the outer coil field.

5.3.1 Normalized B values

In this first paragraph the values of magnetic flux density B will be represented. They are computed on a plane posed at a middle distance between the transmitter and the receiver coil. The representation type is a contour figure, that reports the lines in which the field has the same values.

Circular coil

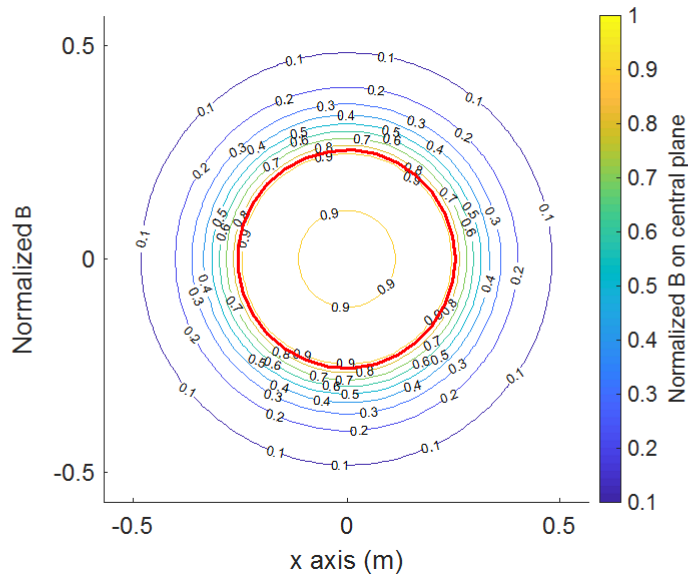


Figure 5.8: Circular coil magnetic flux density contour

In figure it 5.8 it cab be noticed a red circle, this is the middle line of the circular coil. As can be seen the inner field is constant at about the 90% of the maximum field value. Instead the outer field goes gradually down reaching the 10% at about half meters form the coil center. Therefore, between the transmitter and receiver the field is high and this behavior justify the high coupling value obtained by this geometry.

Rectangular coil

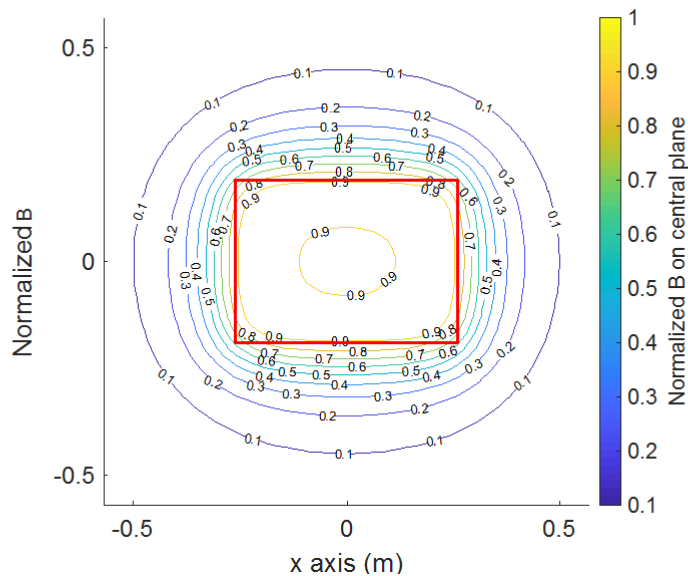


Figure 5.9: Rectangular coil magnetic flux density contour

For the rectangular coil the inner and outer field behavior is quite the same of the circular one, because it is a non-polarized type coil therefore the flux pipe is similar.

Double-D coil

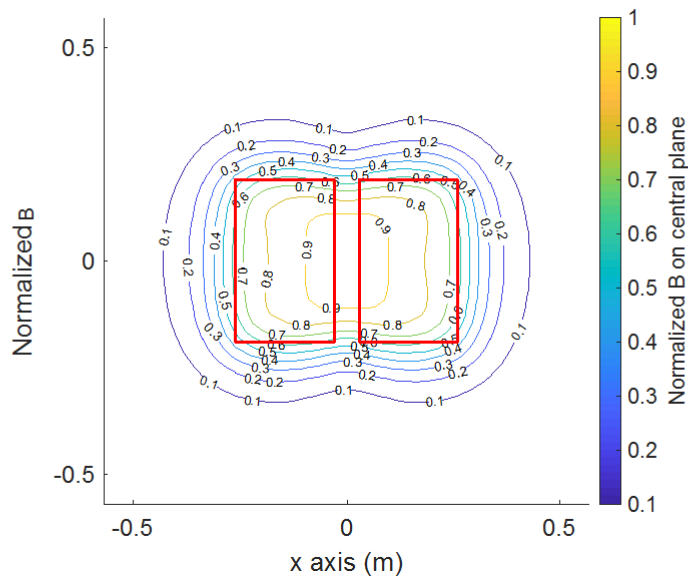


Figure 5.10: Double-D coil magnetic flux density contour

The double-D coil is a polarized type coil. For this coil the flux pipe is driven to go from one "D" to the other, as consequence it can be seen that the outer field is nearer to the coil.

Double-D overlapped receiver coil

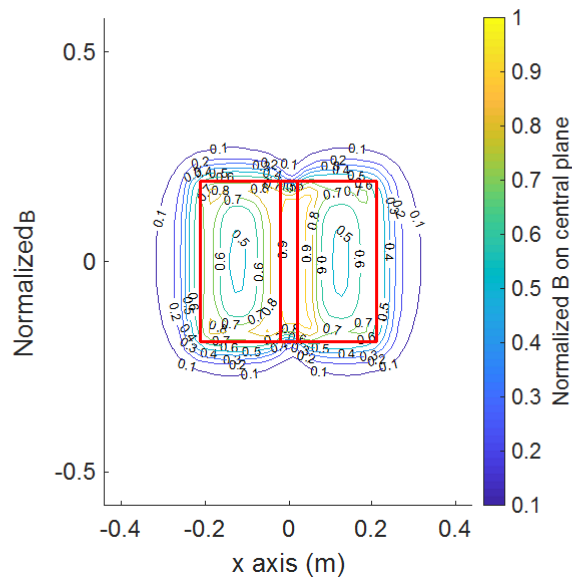


Figure 5.11: Double-D overlapped receiver coil magnetic flux density contour

In this case the overlap allows, with respect to the normal double-D, to further drop down the outer B field. The magnetic field is high between the overlapping zone and about 0.5 to 0.6 inside the D.

Double-D overlapped coil

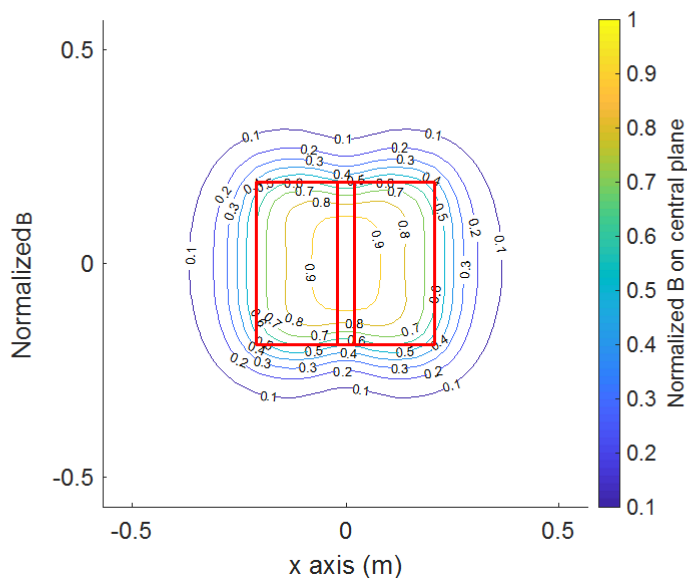


Figure 5.12: Double-D overlapped coil magnetic flux density contour

For this coil type the inner field is higher than the previous, but is better distributed. The outer field seems similar, even if it cannot be appreciated with precision.

Double-D overlapped transmitter coil

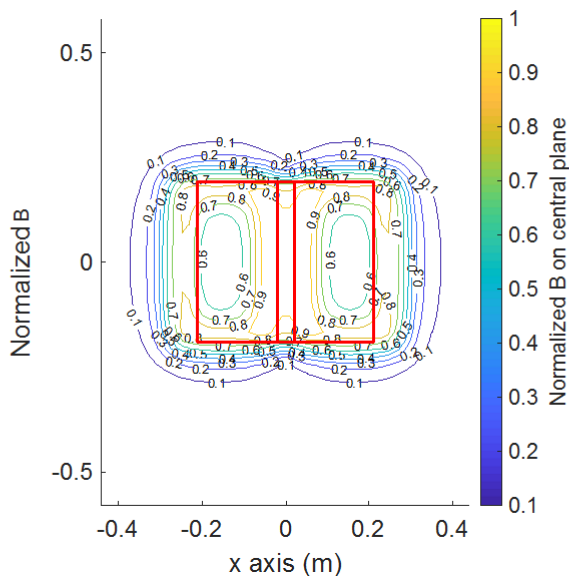


Figure 5.13: Double-D overlapped transmitter coil magnetic flux density contour

The inner field is lower than the previous coil, even if the double-D overlapped at both the transmitter and the receiver has more symmetry and consequently a better shaped inner field.

DDQ coil

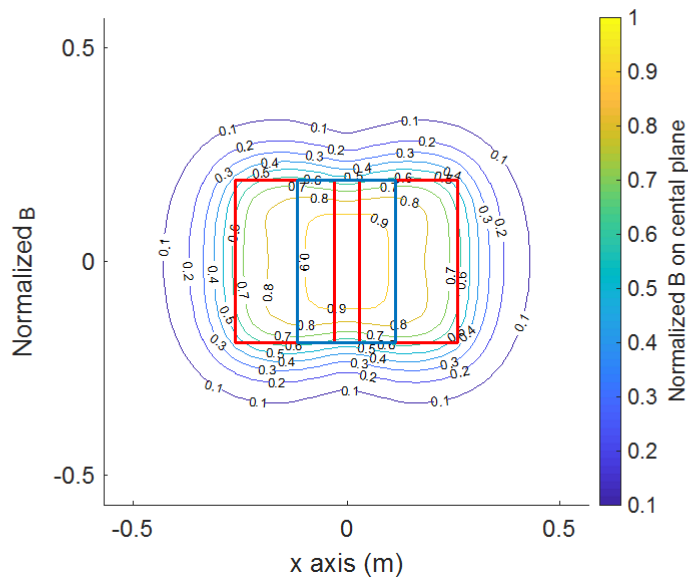


Figure 5.14: DDQ coil magnetic flux density contour

These figure appears equal to the DD coil because the in the quadrature coil enter and exit the same flux line. So, it is not coupled.

DDQ overlapped transmitter coil

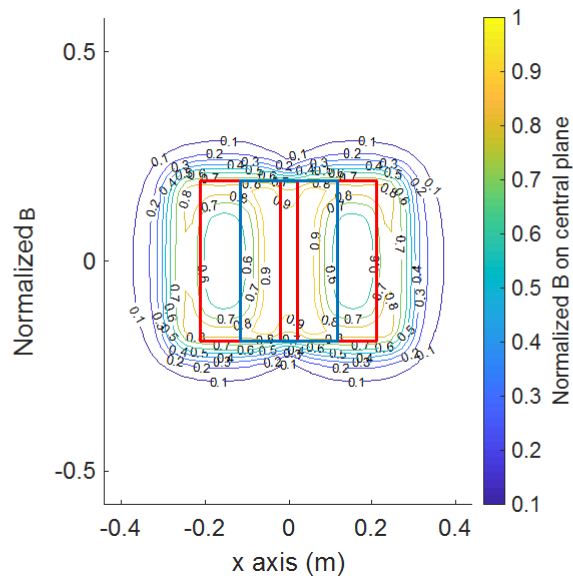


Figure 5.15: DDQ overlapped transmitter coil magnetic flux density contour

This coil has the same field of the DD_{ovtr} coil, because of the same reason quadrature coil.

DDQ overlapped receiver coil

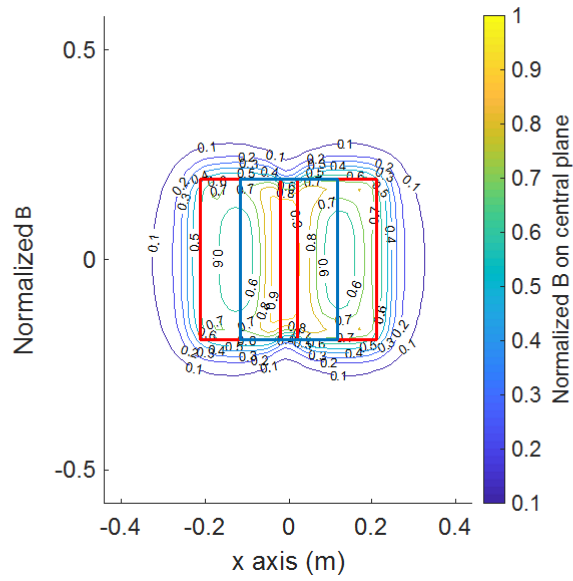


Figure 5.16: DDQ overlapped receiver coil magnetic flux density contour

This coil has the same field of the DD_{ovrec} for the same reason.
DDQ overlapped receiver and transmitter coil

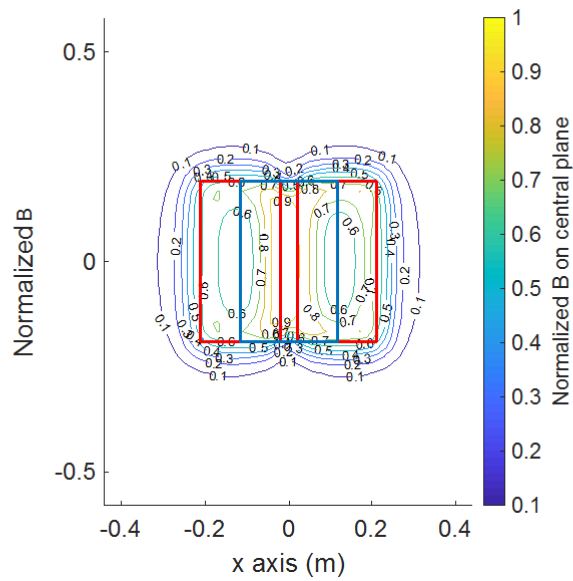


Figure 5.17: DDQ overlapped receiver and transmitter coil magnetic flux density contour

This coil has the same field of The $DD_{ovtrrec}$

5.3.2 B field on x direction transmitter plane

In this figure the values of B , computed on the transmitter plane, are superimposed on one figure to compare their behavior on the x direction. fig. 5.18

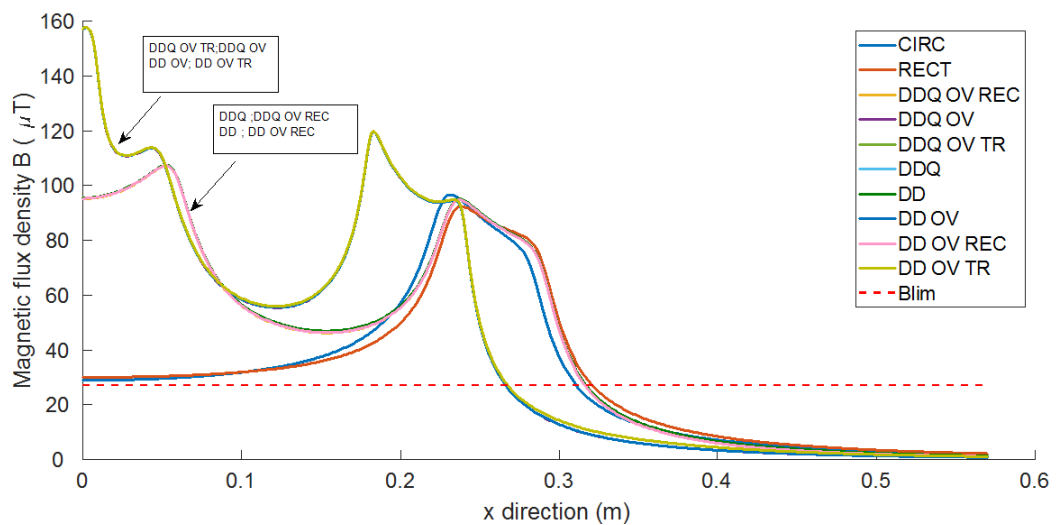


Figure 5.18: Magnetic flux density on x axis (transmitter plane)

Looking at the graph, it can be noticed that some lines are superimposed, for this reason three main groups can be distinguished. The non-polarized coils (rectangular and circular) have a slightly higher value of field with respect to the B limit in the coil center. Reach their maximum on the coil wire and goes under the rectangular coil goes under the limit before than the circular one.

The first group of coil (green) has its highest value of field in the coil center at about $160 \mu\text{T}$. Moreover it present a second further pick of $120 \mu\text{T}$ at around 0.2 m and goes under the coil limit before of a distance of 0.3 m from the coil center.

The second group (pink), has an intermediate situation. These coils have value of about $100 \mu\text{T}$ in the coil center and reach the highest value at about 0.05 m . The field goes under $27 \mu\text{T}$ after 0.3 m .

A bar chart is representd to clearly identify the distance to which each coils goes under the B limit of $27 \mu\text{T}$, indicated with a dashed red line in the precious figure.

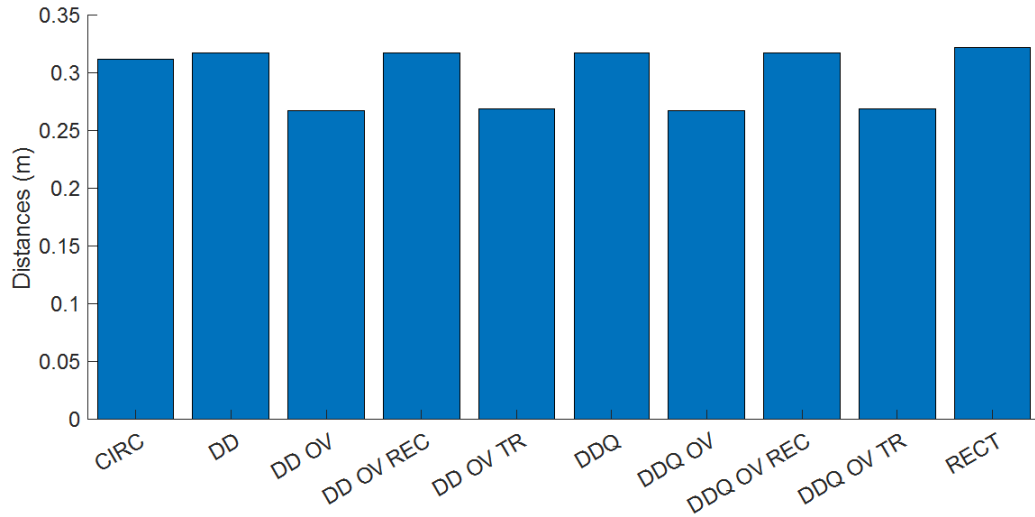


Figure 5.19: Distances at which each geometry reach field limit (transmitter plane)

In this figure a pair of interesting data can be noticed: the geometries with the overlapped transmitter and both overlapped transmitter and receiver go under the limit value at about 0.27 m. All the others figures are up to 0.3 m with the circular coil that has a slightly lower distance.

5.3.3 B field on x direction central plane

In this paragraph the same results of the previous section are reported, but for the central plane. First, it will be analyzed the plot-line figure:

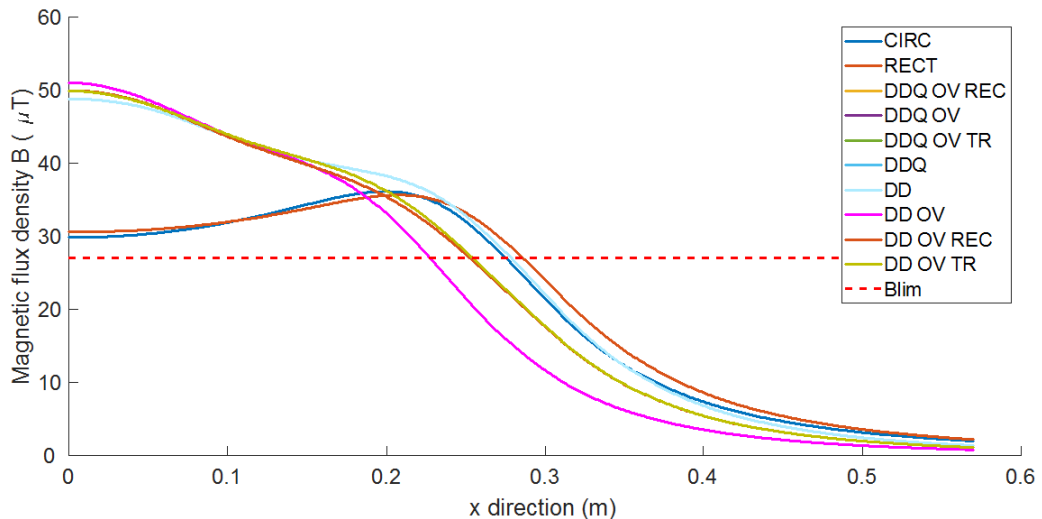


Figure 5.20: Magnetic flux density on x axis (central plane)

In this figure the overall field values are lower than the previous figure. In fact, the group of polarized coils have their maximum value in the coil center at about 50 µT. But each geometry goes under the limit value at different distances. The non polarized coils have about 30 µT in the coil center and goes about 3.6 µT in proximity of the coil wire.

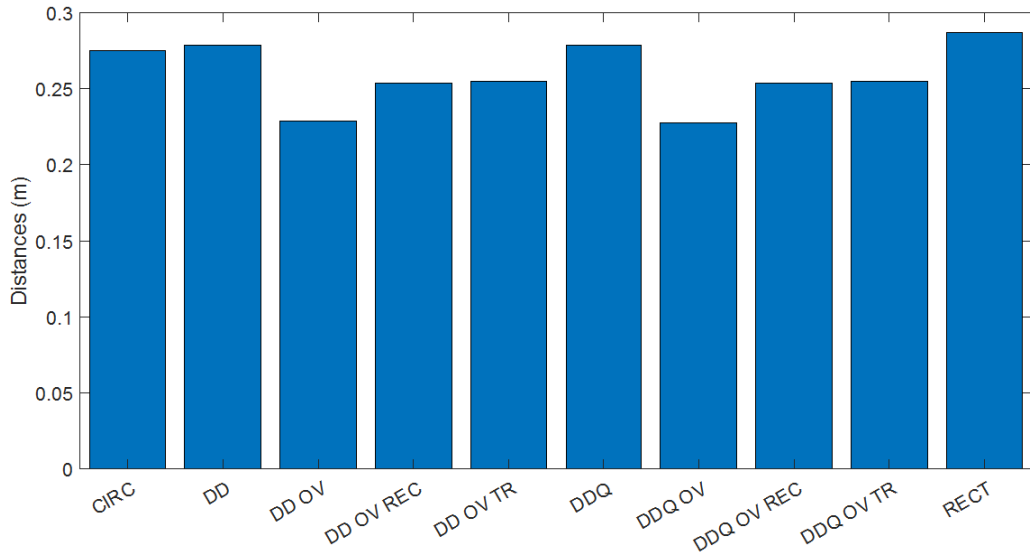


Figure 5.21: Distances at which each geometry goes under the field limit (central plane)

The DD_{OV} and DDQ_{OV} reach the limit B value at the lower distance (about 0.23 m) than the others geometries. The DDQ_{OVREC} , DDQ_{OVTR} , DDQ_{OVREC} and DDQ_{OVTR} have a medium behavior reaching the limit at a distance of 0.25 m. The rectangular coil has the highest distance at about 0.28 m.

5.3.4 B field on x direction receiver plane

In this section the same analysis will be carried out for the receiver plane.

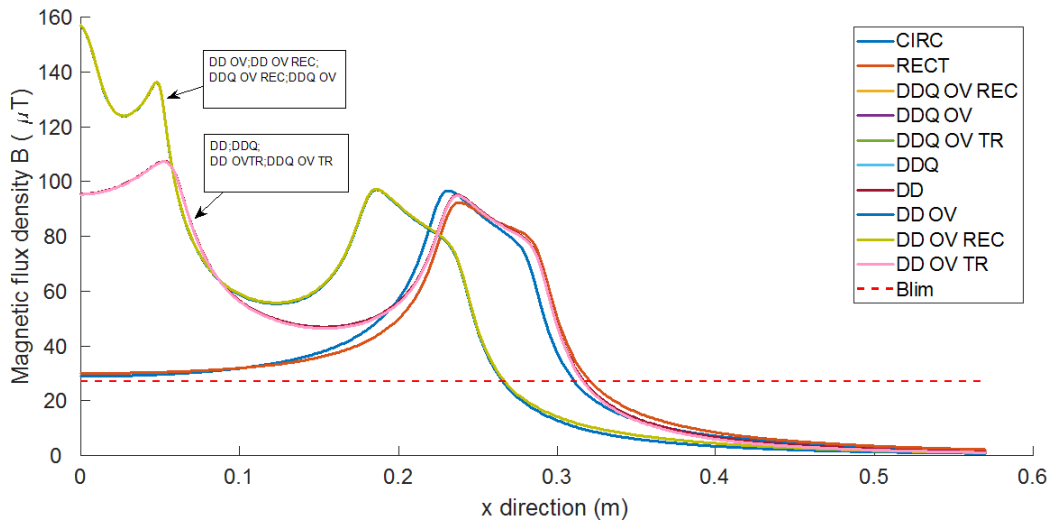


Figure 5.22: Magnetic flux density on x axis (receiver plane)

In the coil center the DD_{OVREC} , DD_{OV} DDQ_{OV} and DDQ_{OVREC} have the highest field value of about 160 μT . At the same point the coils DD , DDQ , DD_{OVTR} and DDQ_{OVTR} have a value of about 90 μT . The non polarized coils remain with the same value of about 30 μT . DD_{OVREC} , DD_{OV} DDQ_{OV} and DDQ_{OVREC} coils are both

well detached from the others geometries they goes under the field limit largely before the others.

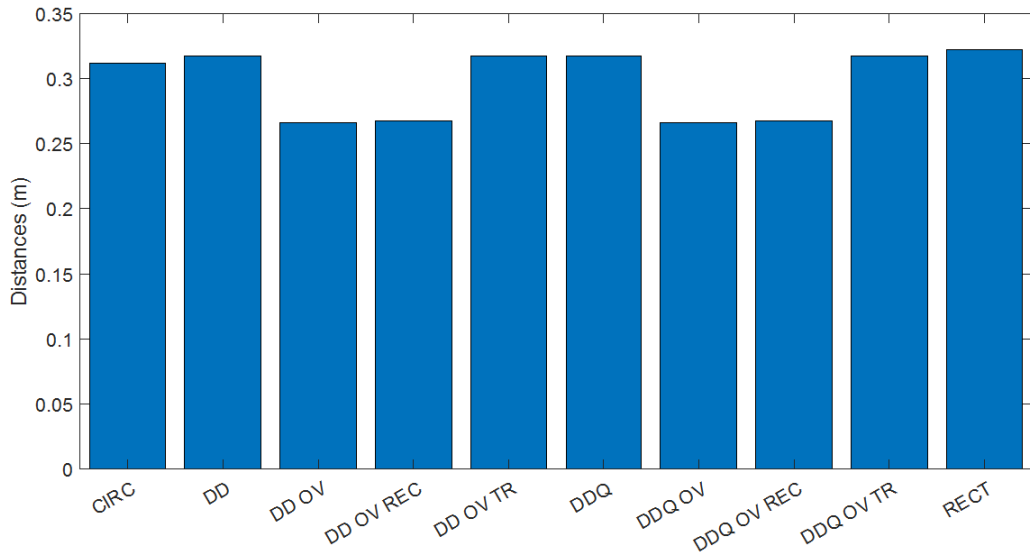


Figure 5.23: Distances at which each geometry reach the field limit (receiver plane)

This figure highlight the same behavior that have been seen for the receiver plane. In fact, in this case the receiver overlapped DDQ_{OVREC} , DD_{OVREC} , $DDOV$ and $DDQOV$ reach the field limit for the smallest distance of about 0.26 m. Instead the overlapped transmitter (DD_{OVTR} and DDQ_{OVTR}) and DDQ and DD coil have a lower performance. They reach the field limit at about 0.32 m.

5.3.5 B field on y direction transmitter plane

In this section the magnetic flux field value will be presented, but this time on the y direction.

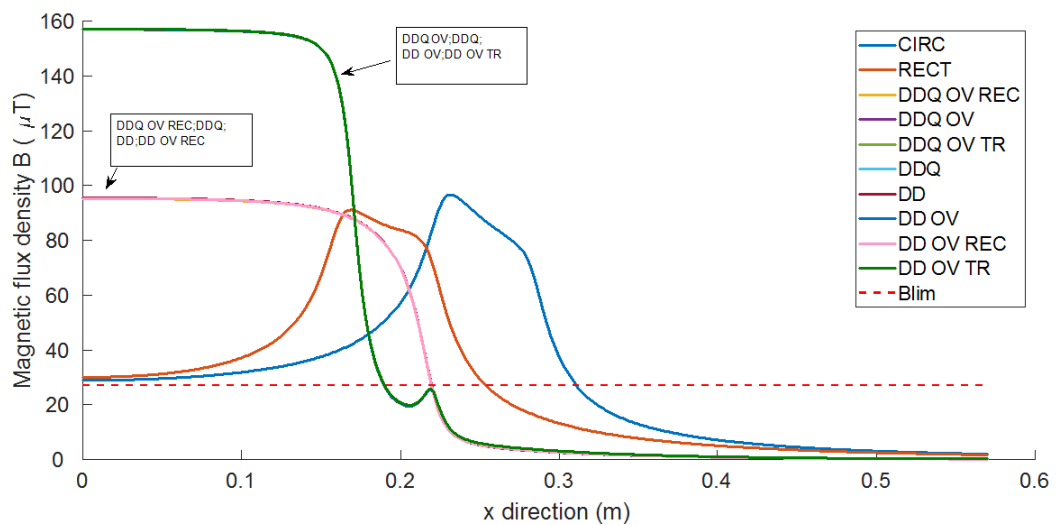


Figure 5.24: Magnetic flux density on y axis, transmitter plane

Looking at the figure 5.24 three groups of coils can be distinguished. The first group ($DDQOV, DDQOVTR, DDOV, DDOVTR$) have the highest value in the coil center at about $160 \mu\text{T}$. The second group ($DDQOVREC, DDQ, DDOVREC, DD$) maintain a constant value of $90 \mu\text{T}$ inside the coil area. The unipolar coils start from about $30 \mu\text{T}$. In proximity of the coil edge the polarized geometries fall down and the rectangular reaches its higher value of $90 \mu\text{T}$. The two unipolar coils reach the maximum field at a different distance because the rectangular geometry has its short side on y direction.

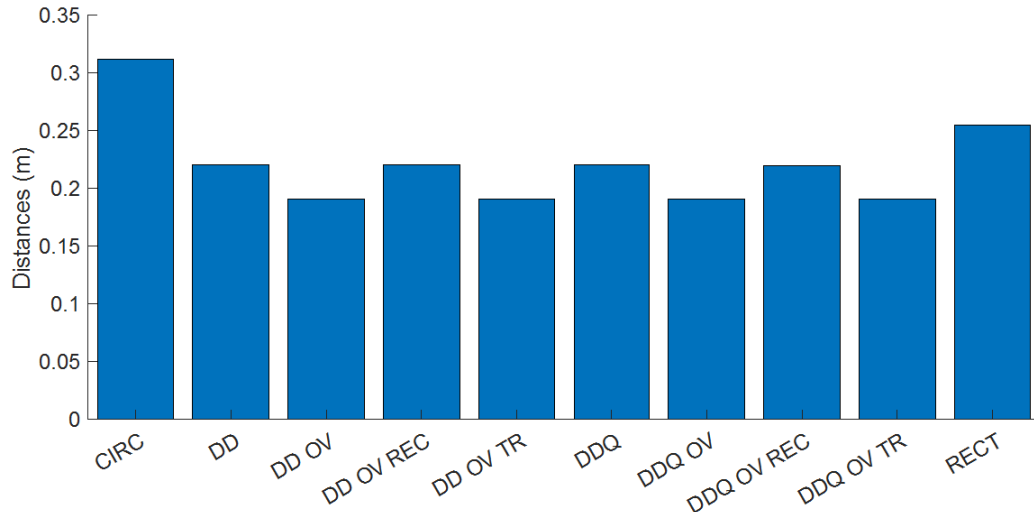


Figure 5.25: Distances at which each geometry reach the field limit (transmitter plane)

Looking at the bar chart 5.25 the previously results are confirmed. There is a big difference between the circular coil and the other coil its goes under the limit value at a distance of 0.32 m.

5.3.6 B field on y direction central plane

Field values on y direction for the central plane.

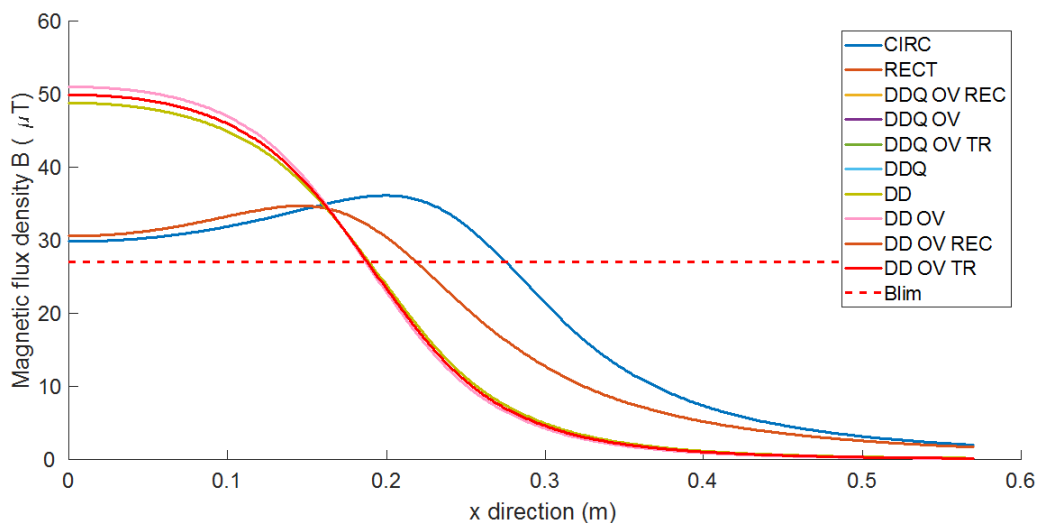


Figure 5.26: Magnetic flux density on y axis (central plane)

In fig. 5.26 the unipolar and polarized coil are well separated. The polarized coils have the same behavior, keep the field constant around the value of $50 \mu\text{T}$ inside the coil. In proximity of the coil edge start to go down. The unipolar coil maintaining the same trend of the previous graphs.

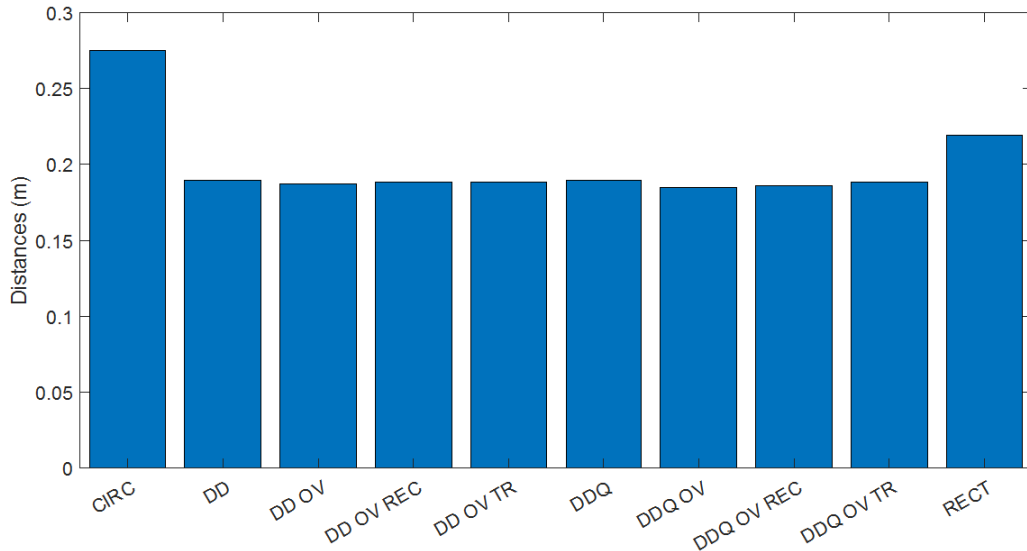


Figure 5.27: Distances at which each geometry reach the field limit (central plane)

The bar chart confirms that the polarized coil goes under the field limit at a distance of 0.18 m from the coil center. The rectangular at 0.22 m and the circular at 0.28 m.

5.3.7 B field on y direction receiver plane

In this paragraph the results on y directions for the receiver plane will be showed.

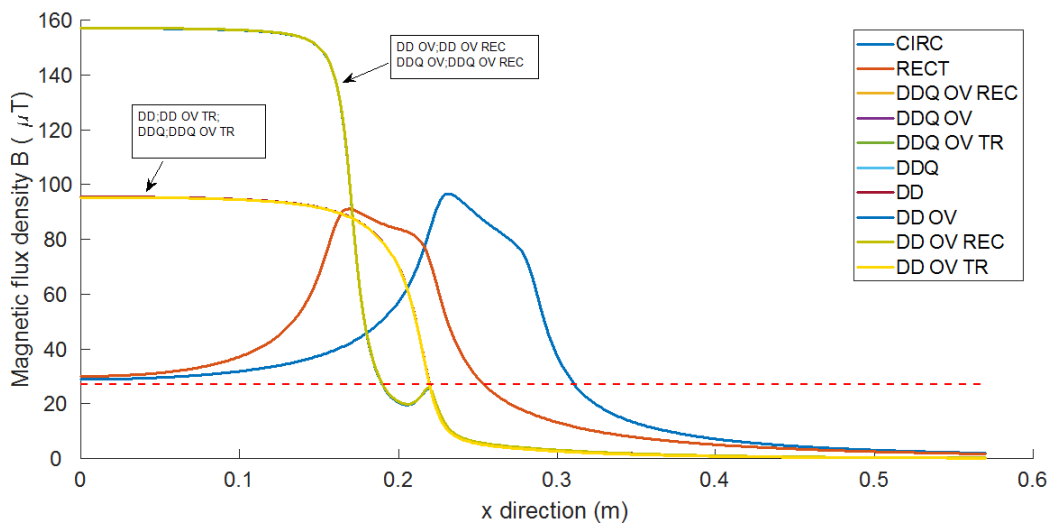


Figure 5.28: Magnetic flux density on y axis (receiver plane)

In figure 5.28 it can be noticed on this plane the group of coil with the receiver and

both transmitter and receiver overlapped have less stray field outside the coil area. In fact, they reach the limit value before than the second group of polarized coils.

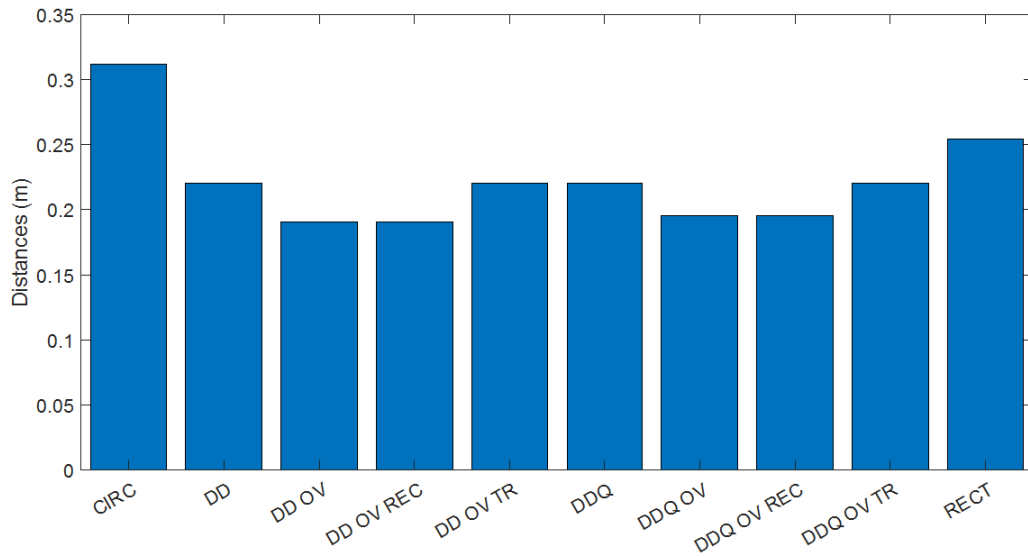


Figure 5.29: Distances at which each geometry reach the field limit (receiver plane)

The geometries with the overlapped receiver and both the transmitter and receiver reach the field limit at 0.18 m from the coil center. While the circular geometry still has the higher value of 0.32 m.

5.4 3D B field representation on x-z and y-z planes

For the sake of completeness in this section the magnetic flux density representation on the x-z and y-z planes are showed.

Circular geometry

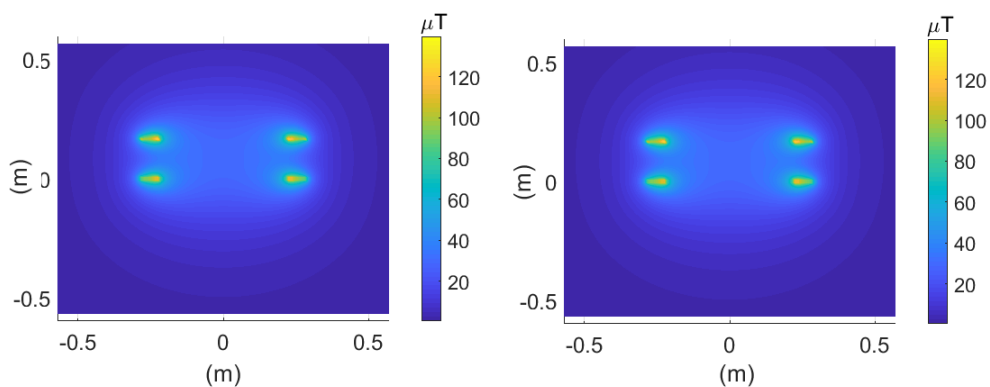


Figure 5.30: Magnetic flux density on x-z and y-z planes (circular coil)

Rectangular geometry

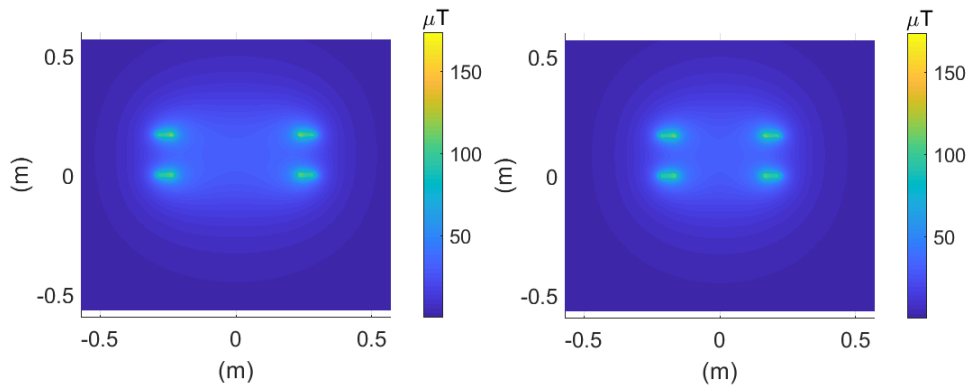


Figure 5.31: Magnetic flux density on x-z and y-z planes (rectangular coil)

Double-D geometry

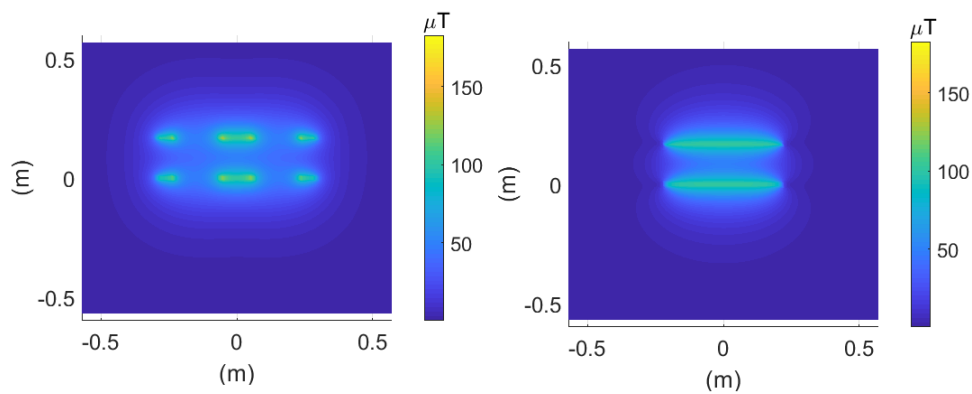


Figure 5.32: Magnetic flux density on x-z and y-z planes (double-D coil)

Double-D overlapped receiver geometry

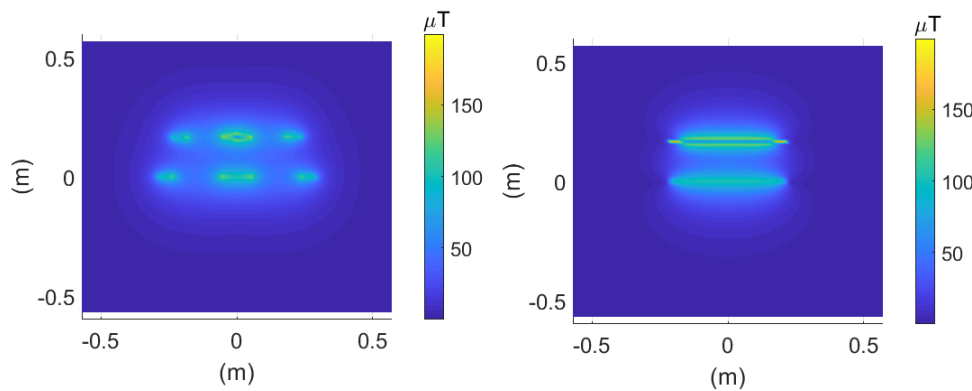


Figure 5.33: Magnetic flux density on x-z and y-z planes (DD_{OVREC} coil)

Double-D overlapped receiver and transmitter geometry

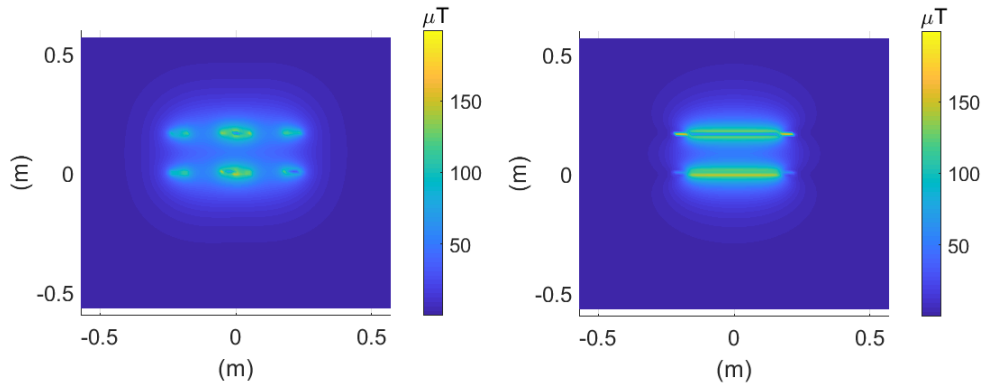


Figure 5.34: Magnetic flux density on x-z and y-z planes ($DD_{OVRECTR}$ coil)

Double-D overlapped transmitter geometry

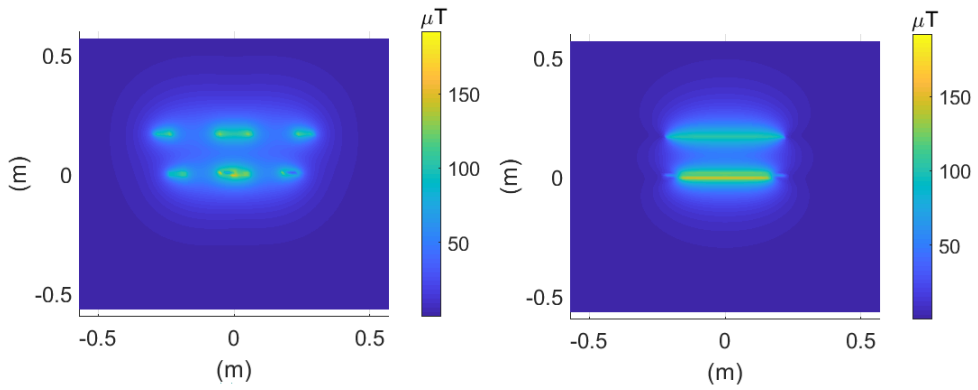


Figure 5.35: Magnetic flux density on x-z and y-z planes (DD_{OVTR} coil)

For the no-misalignment condition there is no current in the quadrature coil. For this reason the DDQ will have the same field of DD , the DD_{OV} of the DDQ_{OV} , the DDQ_{OVREC} of the DD_{OVREC} and the DDQ_{OVTR} of the DD_{OVTR} .

Chapter 6

Conclusion

The presented conclusion are divided according to the the two adopted parameters for the comparison

6.1 Coupling factor k

Considering this parameter the results show that for the no-misalignment condition unipolar geometries have a higher value of k than the polarized geometries. In particular, the circular coil coupling factor is higher than the rectangular one. Among the polarized coils the DD_{OV} and DDQ_{OVTR} reach to two highest value.

This result remains valid also for variation of the air-gap. In fact, at the maximum air-gap, the above mentioned coils maintain the highest values of k . For what concern along x the results shows that the circular geometry loses coupling quite soon, while the rectangular behaves in a better way. The polarized coils have a better in misalignment condition. The DD and the DD_{OVREC} are significantly robust to to x misalignment along x , keeping a good slope. Along the y misalignment all the rectangular type coils behave in the same way. The circular seems to have a better performance, this is due to the fact that on the y direction the rectangular type coils present their short edge.

6.2 Magnetic flux density B

The magnetic flux density results show, as general behavior, that the polarized coils maintain a lower outer field values with respect to the unipolar ones. This because their capacity to guide the flux from one pole to the other, limiting the stray field. In fact both the polarized coil types go under the B limit of 27 μT for higher distances with respect to the polarized coils. This part of the study has highlighted the importance of the overlap. When the overlap is applied to both transmitter and receiver good low stray field can be obtained on each of the three analyzed planes.

In conclusion, the unipolar coils are suitable for those application in which the system is expected to work near the no misalignment condition. This applies especially for the circular geometry. The rectangular coil is a good compromise between the values of k and the misalignment behavior.

The polarized coil have the advantages to lose less coupling than the unipolar one with respect to the misalignment presenting low stray field as well. Moreover, they have the possibility to overlap the coils allowing allowing a separated control for each coil.

Regarding to the magnetic flux density B the polarized coils have surely a better behavior than the unipolar ones. Moreover, when they are overlapped, the field goes under the the limit of B before than a normal polarized coil.

This characteristics can be further exploited to improve the performance of the IPT. These simulations can be carried out adding bars of ferrite and an aluminum plate. This does not modify the found conclusion because the coils behavior depends substantially on their geometry.

Appendix A

Appendix

In this appendix will be showed the procedure carried out on Matlab to calculate the system inductances, the coupling factor k and the magnetic flux density B .

Coupling factor In this section will be showed the procedure used for the double-D coil. In order to calculate the coupling coefficient k , first is drawn the coil geometry using a customized Matlab function "cretecoil3d". This one, receiving a set of points, creates a solid coil bringing together a series of 3d elementary solids.

```
coil1 = createCoil3d(C1,P1,I1,'obj',3);  
coil2 = createCoil3d(C2,P2,I2,'obj',3);  
coil3 = createCoil3d(C3,P3,I3,'obj',3);  
coil4 = createCoil3d(C4,P4,I4,'obj',3);
```

having the coil geometry the vector potential for each coil can be computed:

```
% vector potential functions  
Afun1 = @(Q) coilVectorPotential3d(coil1,Q,'method','full');  
Afun2 = @(Q) coilVectorPotential3d(coil2,Q,'method','full');  
Afun3 = @(Q) coilVectorPotential3d(coil3,Q,'method','full');  
Afun4 = @(Q) coilVectorPotential3d(coil4,Q,'method','full');
```

all the energies related with each self and mutual inductance are calculated:

```

%energies
W11 = coilMagneticEnergy3d(coil1,Afun1);
W12 = coilMagneticEnergy3d(coil1,Afun2);
W21 = coilMagneticEnergy3d(coil2,Afun1);
W22 = coilMagneticEnergy3d(coil2,Afun2);
W13 = coilMagneticEnergy3d(coil1,Afun3);
W31 = coilMagneticEnergy3d(coil3,Afun1);
W33 = coilMagneticEnergy3d(coil3,Afun3);
W23 = coilMagneticEnergy3d(coil2,Afun3);
W32 = coilMagneticEnergy3d(coil3,Afun2);
W14 = coilMagneticEnergy3d(coil1,Afun4);
W41 = coilMagneticEnergy3d(coil4,Afun1);
W44 = coilMagneticEnergy3d(coil4,Afun4);
W24 = coilMagneticEnergy3d(coil2,Afun4);
W42 = coilMagneticEnergy3d(coil4,Afun2);
W34 = coilMagneticEnergy3d(coil3,Afun4);
W43 = coilMagneticEnergy3d(coil4,Afun3);

```

once all the energies have been obtained the relative inductances can be computed:

```

%induttanze
L11 = 2*W11/I1^2;
L12 = 2*W12/(I1*I2);
L21 = 2*W21/(I2*I1);
L22 = 2*W22/I2^2;
L13 = 2*W13/(I1*I3);
L31 = 2*W31/(I3*I1);
L33 = 2*W33/I3^2;
L23 = 2*W23/(I2*I3);
L32 = 2*W32/(I3*I2);
L14 = 2*W14/(I1*I4);
L41 = 2*W41/(I4*I1);
L44 = 2*W44/I4^2;
L24 = 2*W24/(I2*I4);
L42 = 2*W42/(I4*I2);
L34 = 2*W34/(I3*I4);
L43 = 2*W43/(I4*I3);

```

in the end, are defined the equivalent transmitter and receiver inductances and the coupling coefficient k can be computed:

```

Leq_t = L11+L21+L21+L22;
Leq_r = L33+L43+L34+L44;
M_tr = L13+L23+L14+L24;
M_rt = L31+L41+L32+L42;

k = M_tr/sqrt(Leq_t*Leq_r);

```

Magnetic flux density B

In this section will be reported the procedure to calculation the magnetic flux density on each of the previously discussed planes.

```
x_t = linspace(2*(-Rext_t),2*Rext_t,60);
y_t = linspace(2*(-Rext_t),2*Rext_t,60);
z_t = 4*h_t;
x_c = linspace(2*(-Rext_t),2*Rext_t,60);
y_c = linspace(2*(-Rext_t),2*(Rext_t),60);
z_c = zCoil/2;
x_r = linspace(2*(-Rext_t),2*Rext_t,60);
y_r = linspace(2*(-Rext_t),2*Rext_t,60);
z_r = zCoil-(4*h_r);
```

given the x-y-z coordinates, in array of 60 points, thanks to the "meshgrid" matlab function a 60x60 grid of points is created. This process is re-iterated for each plane.

```
[X_t,Y_t,Z_t] = meshgrid(x_t,y_t,z_t);
[X_c,Y_c,Z_c] = meshgrid(x_c,y_c,z_c);
[X_r,Y_r,Z_r] = meshgrid(x_r,y_r,z_r);
```

obtained the meshgrid points these are ordered in a a matrix to obtain the the field valuse on the three dimensions. Then each coil contribution to each plane is computed and added up to compute the actual field for each plane. Then, knowing the magnetic permeability μ_0 and using the relation: $B = \mu_0 H$ the magnetic flux density is computed.

```
H_t=coilMagneticField3d(coil1,Q_t);
H_tr=coilMagneticField3d(coil1,Q_r);
H_ct=coilMagneticField3d(coil1,Q_c);
H_cr=coilMagneticField3d(coil2,Q_c);
H_r=coilMagneticField3d(coil2,Q_r);
H_rt=coilMagneticField3d(coil2,Q_t);

Heq_t=H_t+H_rt;
Heq_r=H_r+H_tr;
H_ctr=H_cr+H_ct;

Beq_t=Mu0*Heq_t;
B_ctr=Mu0*H_ctr;
Beq_r=Mu0*Heq_r;
```

the magnitude of the field vectors is computed and reshaped to match the plane dimensions:

```

Bt_abs=sqrt (sum (abs (Beq_t) .^2,2));
Bc_abs=sqrt (sum (abs (B_ctr) .^2,2));
Br_abs=sqrt (sum (abs (Beq_r) .^2,2));

```

```

Bt=reshape (Bt_norm, [60,60]);
Bc=reshape (Bc_norm, [60,60]);
Br=reshape (Br_norm, [60,60]);

```

Line field

A similar procedure is used for the plot-line field.

First arrays of 500 points are created:

```

% plotline field
if graph == 1
x_t_line = linspace(0,2*Rext_t,500);
y_t_line = 0*ones(1,500);
z_t_line = 4*h_t*ones(1,500);
x_c_line = linspace(0,2*Rext_t,500);
y_c_line = 0*ones(1,500);
z_c_line = zCoil/2*ones(1,500);
x_r_line = linspace(0,2*Rext_t,500);
y_r_line = 0*ones(1,500);
z_r_line = (zCoil-4*h_r)*ones(1,500);
end
if graph==2
x_t_line = 0*ones(1,500);
y_t_line = linspace(0,2*Rext_t,500);
z_t_line = 4*h_t*ones(1,500);
x_c_line = 0*ones(1,500);
y_c_line = linspace(0,2*(Rext_t),500);
z_c_line = zCoil/2*ones(1,500);
x_r_line = 0*ones(1,500);
y_r_line = linspace(0,2*Rext_t,500);
z_r_line = (zCoil-4*h_r)*ones(1,500);
end

```

As it for the planes field, every coil contribute to the magnetic field is computed added up to obtain the actual field. After, the B magnitude is computed.

```

H_t_line=coilMagneticField3d(coil1,Q_t_line);
H_tr_line=coilMagneticField3d(coil1,Q_r_line);
H_ct_line=coilMagneticField3d(coil1,Q_c_line);
H_cr_line=coilMagneticField3d(coil2,Q_c_line);
H_r_line=coilMagneticField3d(coil2,Q_r_line);
H_rt_line=coilMagneticField3d(coil2,Q_t_line);

Heq_t_line=H_t_line+H_rt_line;
Heq_r_line=H_r_line+H_tr_line;
Heq_tr_line=H_cr_line+H_ct_line;

Beq_t_line=Mu0*Heq_t_line;
Beq_tr_line=Mu0*Heq_tr_line;
Beq_r_line=Mu0*Heq_r_line;

Btline_abs=sqrt(sum(abs(Beq_t_line).^2,2));
Bcline_abs=sqrt(sum(abs(Beq_tr_line).^2,2));
Brline_abs=sqrt(sum(abs(Beq_r_line).^2,2));

```

Bibliography

- [1] V. Cirimele, “Design and integration of a dynamic ipt system for automotive applications,” Master’s thesis, Politecnico di Torino and Université Paris-Saclay, 2017.
- [2] V. Cirimele, F. Freschi, and M. Mitolo, “Inductive power transfer for automotive applications: State-of-the-art and future trends,” in *Industry Applications Society Annual Meeting, 2016 IEEE*, pp. 1–8, IEEE, 2016.
- [3] Z. Bi, T. Kan, C. C. Mi, Y. Zhang, Z. Zhao, and G. A. Keolelian, “A review of wireless power transfer for electric vehicles: Prospects to enhance sustainable mobility,” *Applied Energy*, vol. 179, pp. 413–425, 2016.
- [4] M. Budhia, G. A. Covic, and J. T. Boys, “Design and optimization of circular magnetic structures for lumped inductive power transfer systems,” *IEEE Transactions on Power Electronics*, vol. 26, pp. 3096–3108, Nov 2011.
- [5] A. Tejada, C. Carretero, J. T. Boys, and G. A. Covic, “Ferrite-less circular pad with controlled flux cancelation for ev wireless charging,” *IEEE Transactions on Power Electronics*, vol. 32, no. 11, pp. 8349–8359, 2017.
- [6] R. Bosshard and J. W. Kolar, “Multi-objective optimization of 50 kw/85 khz ipt system for public transport,” *IEEE Journal of Emerging and Selected Topics in Power Electronics*, vol. 4, no. 4, pp. 1370–1382, 2016.
- [7] R. Bosshard, U. Iruretagoyena, and J. W. Kolar, “Comprehensive evaluation of rectangular and double-d coil geometry for 50 kw/85 khz ipt system,” *IEEE Journal of Emerging and Selected Topics in Power Electronics*, vol. 4, no. 4, pp. 1406–1415, 2016.
- [8] M. G. Pearce, H. Gao, A. Ramadugu, G. A. Covic, and J. T. Boys, “Robust double d topology for roadway ipt applications,” *2017 IEEE Energy Conversion Congress and Exposition (ECCE)*, pp. 2734–2741, 2017.
- [9] G. A. Covic, M. L. Kissin, D. Kacprzak, N. Clausen, and H. Hao, “A bipolar primary pad topology for ev stationary charging and highway power by inductive coupling,” in *Energy Conversion Congress and Exposition (ECCE), 2011 IEEE*, pp. 1832–1838, IEEE, 2011.
- [10] W. Zhang, J. C. White, A. M. Abraham, C. C. Mi, *et al.*, “Loosely coupled transformer structure and interoperability study for ev wireless charging systems,” *IEEE Trans. Power Electron.*, vol. 30, no. 11, pp. 6356–6367, 2015.

- [11] G. R. Nagendra, G. A. Covic, and J. T. Boys, “Sizing of inductive power pads for dynamic charging of evs on ipt highways,” *IEEE transactions on transportation electrification*, vol. 3, no. 2, pp. 405–417, 2017.
- [12] S. International, “Surface vehicle information report,” tech. rep., SAE International, November 2017.
- [13] F. Rana, “Ece 303 – cornell university,” 2007.